Deliverable 3.4
Multi-physics model extended to a matrix of NWs

PiezoMAT Deliverable 3.4 Multi-physics model extended to a matrix of NWs PiezoMAT – 2017-06-08 D3.4 v1	
Contractual delivery date:	30/06/2017
Actual delivery date:	08/06/2017
Author(s):	R. Dauksevicius
Internal reviewer(s):	V. Lebedev

RESTRICTED DISSEMINATION

EXECUTIVE SUMMARY

This document summarizes the results of finite element (FE) modeling of vertically-aligned ZnO NW arrays including surrounding chip components (seed/top/encapsulating layers and electrodes), taking into account the electrical influence of the external capacitive circuit that imitates readout electronics of the fingerprint sensor. Different versions and alternatives of FE models, characterized by varying degree of structural, electrical, physical and dimensional complexity, were successfully implemented: starting from an idealized piezoelectric model of unencapsulated NW array to the most realistic and adaptive fully-coupled piezoelectric-semiconducting-circuit model of the encapsulated NW array that, which can be readily tailored to the required multi-NW configuration. The configuration of the most realistic "chip-based" piezo-semiconductive model corresponds to the PiezoMAT chip layout that was used for the DEMO3 fabrication. The availability of different model versions and alternatives allowed effective and efficient tackling of specific computationally-intensive simulation tasks by ensuring reasonable solution times and consistent numerical convergence. Systematic parametric studies were conducted with different models, which enabled prediction of electro-mechanical responses of the NWs under different mechanical loading conditions and input system parameters such as NW morphologies, electrode topologies, structural chip configurations, material properties, mechanical coupling conditions at NW/polymer interface, etc. The predictions served as useful inputs during sensor design workflow and allowed to gain deeper understanding about the electro-mechanical behavior of the dynamically deformed ZnO NWs. Reported simulation results were successfully correlated to the experimental results obtained both within the consortium and by other research groups. Good agreement between the numerical and reported experimental values (both absolute and relative, e.g. voltage sensitivities, current densities) validated the predictive credibility of the developed numerical models.

REVISION HISTORY

Revision	Date	Description	Author
V1	08/06/2017	The first draft	R. Dauksevicius

Table of content

1 Introduction

Deliverable **D3.4** is the 4th deliverable in **WP3** (Specifications, models and layouts). This work package comprises the main tasks devoted to fingerprint sensor design along with preliminary technological developments and test/characterization activities within the **PiezoMAT** project. WP3 provides all the elements for dimensioning the addressable ZnO nanowire (NW) arrays, i.e. defining its specifications in terms of topography and expected performance based on predictions of theoretical models and preliminary experimental work. It is determining in a sense that it establishes the layouts of the future PoC (proof of concept) and DEMO (partial demonstrator) chips, which will impact all subsequent process developments.

The WP3 concentrates on the preliminary studies of three basic chip designs (1.1.3.2 of DoW). Among them, option 1 is not intended for wafer-scale chip processing but as a proof-of-concept and supporting object for model validation purposes. Options 2 & 3 should be designed and realized for both PoC and DEMO chip designs with the priority set on option 3. In option 2, four metal contacts are deposited along the perimeter of an ordered array of ZnO NWs and near their clamped extremity. Here, the NW matrix will be encapsulated in a polymer layer to allow deformation transfer. In option 3, NWs of an ordered array will be contacted by a patterned electrode at their bottom section and by a continuous electrode at their top section. Interspace between electrodes will be filled with a polymer similar to the option 2.

Within WP3, tasks 3.1-3.5 focus on device design, tasks 3.4-3.6 are related to the development of piezoelectric models for device design optimization, and tasks 3.7-3.10 are devoted to the preliminary technological developments and characterizations for device design optimization.

The tasks reported in D3.4 are listed in Table 1.1.

Table 1.1: Tasks reported in Deliverable D3.4.

Task	*Description*	*Duration*	*Status*
3.6	Multi-NW multi-physics model	M16-M44	Completed

2 Multiphysics finite element modeling of the top-bottom contacted ZnO nanowires for compression force sensing (Option 3)

2.1 Overview of the implemented models (Option 3)

Finite element (FE) modeling activities were pursued in the project with the objectives to provide useful inputs during sensor design workflow and to gain deeper understanding about the electro-mechanical behavior of the dynamically deformed ZnO nanowires (NWs).

Table 2.1.1: Summary of the implemented FE models (Option/Architecture 3).

Version No.	***Type of model***	***Main features***	***Model images***
FEM3.1	*Single/multi-NW piezoelectric models (3D)*	▪ Idealized structural & electrical configuration (classical piezoelectric theory): - ZnO: dielectric. - Electrical contacts: ohmic. - Electrical properties of all dielectric and conducting stack layers accounted for. ▪ No encapsulation.	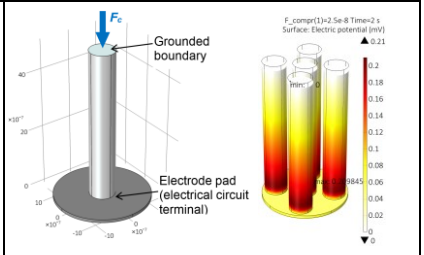
FEM3.2	*Encapsulated multi-NW piezoelectric models (2D)*	▪ 2 alternatives for structural configuration: ▪ Idealized: no multi-layer stack, encapsulated in dielectric polymer. ▪ Realistic (chip-based): with multi-layer stack and encapsulated in dielectric & conducting polymers. ▪ 2 alternatives for mechanical coupling conditions at NW/polymer interface: rigid or contact-based (nonlinear). ▪ Idealized electrical & physical configuration: - ZnO: dielectric. - Electrical contacts: ohmic. - Electrical properties of all dielectric and conducting stack layers accounted for.	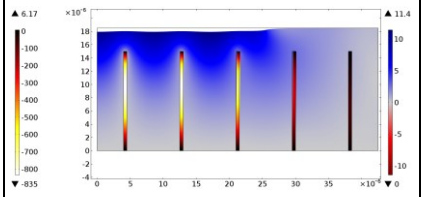
FEM3.3	*Single-NW piezo-semiconductive model (axisymmetric)*	▪ 2 alternatives: with/without encapsulating polymer. ▪ Idealized structural configuration: no multi-layer chip stack. ▪ Realistic electrical & physical configuration: - Coupled piezoelectric & semiconducting properties in ZnO. - Electrical contacts: ohmic or Schottky (nonlinear).	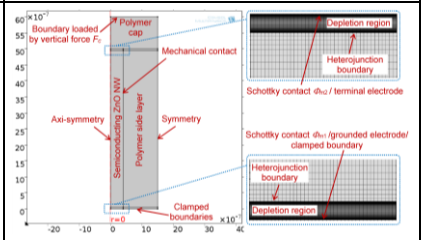
FEM3.4	*Encapsulated single-NW piezo-semiconductive chip-based model (2D)* /directly extendable to NW array/	▪ Realistic structural configuration: NWs integrated on a multi-layer chip stack and encapsulated in dielectric & conducting polymers. ▪ Realistic electrical & physical configuration: - Coupled piezoelectric & semiconducting properties in ZnO. - Electrical contacts: ohmic or Schottky (nonlinear) - Electrical properties of all stack layers accounted for.	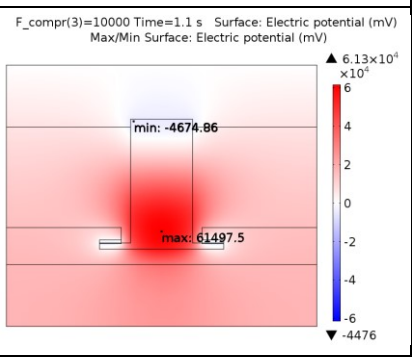

The developed models are classified into two large groups in terms of the modeled sensor "Option" ("Architecture"), which is characterized by a distinct electrical contacting configuration (i.e. electrode topology used for charge collection):

- Option/Architecture 3 (presented in Section 2): a conventional top-bottom contacting option with electrodes that are positioned at the top and bottom NW boundaries. Option 3 NW array is intended for compression force sensing.
- Option/Architecture 2 (presented in Section 3): a more advanced bottom-bottom contacting option with side electrodes that are positioned at the root of a NW. Option 2 NW array is intended for bending force sensing. The side electrodes may be either separated from the NW (suspended) or they may be contacted to it.

A wide range of multiphysics FE models of Option 3 arrayed vertical ZnO NWs were implemented by KTU using COMSOL Multiphysics® software (Table 2.1.1). The NWs were modeled as individually-addressable pressure sensing pixels by connecting them to separate external capacitors, which represented the readout circuitry of the sensor. From a mechanical point of view, the models were treated as quasi-static, while electrically – as dynamic. To deform the NWs, ramping and semi-harmonic loads were used to imitate the actual pressing with a finger and time-dependent numerical studies were performed to predict voltage, charge and current signals generated by each NW.

Different versions of FE models, characterized by varying degree of structural, electrical, physical and dimensional complexity, were successfully implemented: starting from a classical piezoelectric model of unencapsulated NW array (ver. FEM3.1) to the fully-coupled piezoelectric-semiconducting-circuit model of the encapsulated NW array (ver. FEM3.4). The structural configuration of the most complex "chip-based" models (ver. FEM3.2 & FEM3.4) corresponds to the chip layout that was developed in the project and was used for the DEMO3 fabrication. Availability of different model versions allowed to avoid computationally-prohibitive simulations and rationally address modeling challenges associated with the solution convergence of time-dependent multiphysics simulations, particularly in the case of piezo-semiconductive models with nonlinear Schottky contacts (ver. FEM3.4) or models of the encapsulated NW array with nonlinear contact-based mechanical interactions imposed on multiple NW/polymer interfaces (ver. FEM3.2).

Extensive parametric numerical studies were conducted with different model versions and alternatives, which enabled prediction of electro-mechanical responses of the NWs under different mechanical loading conditions and input system parameters (e.g. NW morphologies, electrode topologies, structural chip configurations, material properties, external circuit capacitances, mechanical coupling conditions at NW/polymer and polymer/ridge interfaces, etc.). Modeling and simulation results for model versions FEM3.1 and FEM3.3 were reported in D3.3. Meanwhile, D3.4 focuses on the results obtained with the model versions FEM3.2 and FEM3.4.

2.2 Multi-NW piezoelectric model of the encapsulated Option 3 ZnO NW array (ver. FEM3.2)

2.2.1 Implementation of the structurally-idealized model ver. FEM3.2

COMSOL software was used to develop the structurally-idealized 2D FE models of the encapsulated ZnO NW array (5 piezo-pixels), which is subjected to mechanical loading that imitates pressing with a finger (Figure 2.2.1.1, Table 2.1.1). The *piezo-pixel* refers here to the modelled piezoelectric-dielectric ZnO NW connected to an external capacitor that represents readout electronics of a fingerprint sensor (in the chip-based model implementation the piezo-pixel may also include the associated chip components such as seed, top and electrode layers). When formulating load conditions, we took a fingerprint region that corresponds to a ridge edge and assumed that the ridge presses the first 3 nanowires from the left (referred to as *loaded NWs*) and the remaining 2 NWs on the right are not directly loaded (*unloaded NWs*). Electrical properties of the polymer (and other chip components) were neglected because we focused on mechanical aspects such as deformation transfer and conditions of mechanical contact between the NWs and the polymer or between the ridge and polymer.

The general design target in an ideal case of pure compressive load is that each loaded nanowire (NW1, NW2, NW3) generates the same output signal (as high as possible), i.e. no variability is observed between V_{NW1}, V_{NW2} and V_{NW3} ($\sigma_V = 0$ V). While the unloaded nanowires (NW4, NW5) should not provide any electrical output in the considered load case. In this respect, for evaluation of performance the following characteristics are derived and analysed: voltage mean ($V_m = (V_{NW1} + V_{NW2} + V_{NW3})/3$), which should be maximized and standard deviation σ_V, which should be minimized.

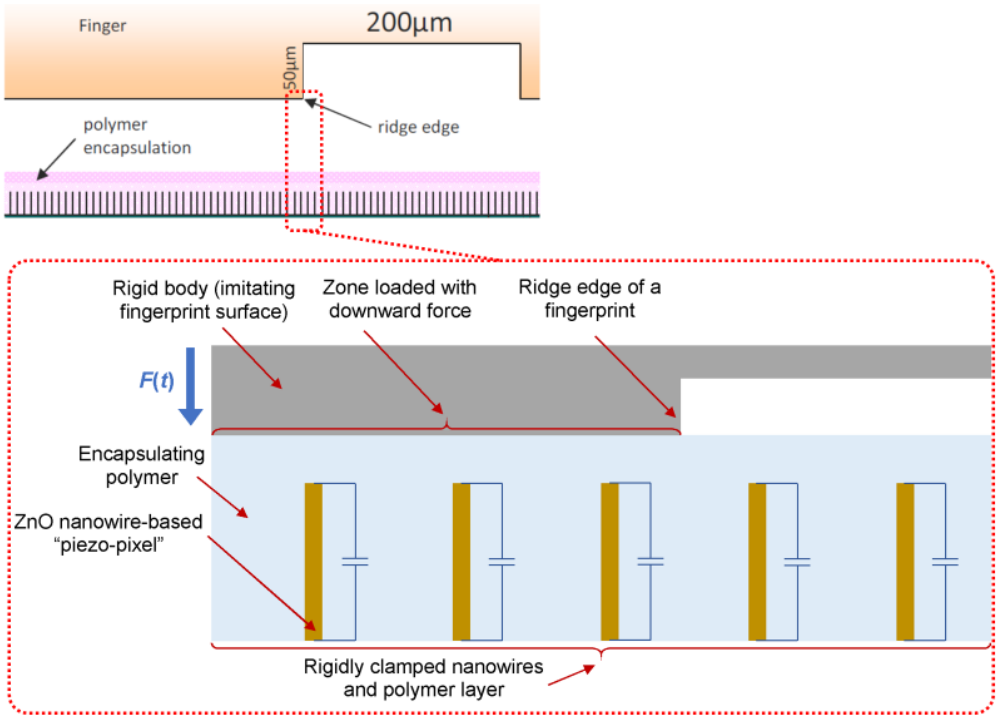

Figure 2.2.1.1: Schematic representation of the modeled encapsulated ZnO NW array, which is deformed by a rigid body that imitates the ridge of a fingerprint.

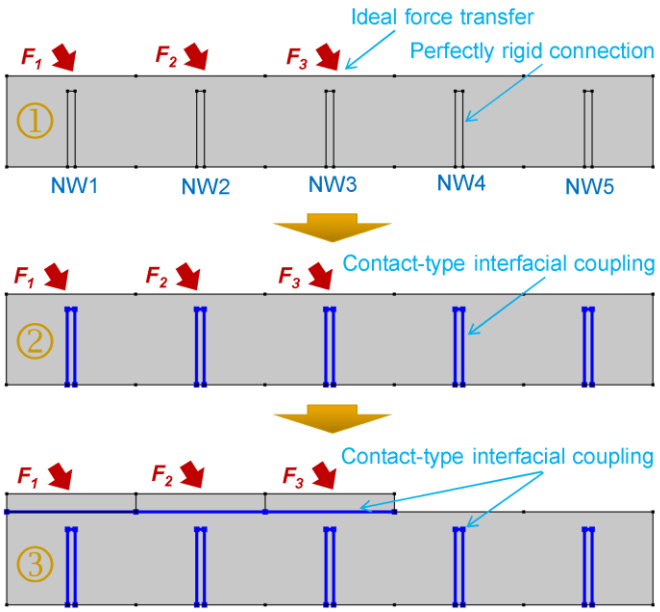

Figure 2.2.1.2: Illustration of the 3 alternatives of the developed FE models ver. FEM3.2.

We have implemented 3 different alternatives of the model ver. FEM3.2 (Figure 2.2.1.2), which are different in terms of mechanical coupling conditions imposed on NW/polymer and ridge/polymer interfaces. The common features of the models:

- ZnO is dielectric and only strain-induced piezoelectric signal is predicted.
- Each NW is connected to an external capacitor of 10 fF (i.e. 5 piezo-pixels).
- Each NW is associated with separate load segment (i.e. 5 segments in this case).
- Segments are loaded with forces F_1, F_2,..,F_n of arbitrary orientation.

The distinctive features of the models:

- Model 1 represents an ideal case when mechanical coupling effects (contact interactions, friction effects) are not considered. In other words, the model assumes a perfect force transfer from the ridge to the encapsulation layer and the NWs are assumed to be rigidly attached to the surrounding polymer (i.e. no gaps, no mechanical slips).
- Model 2 assumes that the NWs are not perfectly rigidly attached to the polymer during deformation process since in reality we could expect detachments of NWs from the polymer layer and the resulting slip effects. Therefore in the model the polymer is separated from the NW by a very small distance and during deformation the polymer undergoes mechanical contact (friction-related effects are not considered at this stage).
- Model 3 additionally assumes that the force transfer from the ridge to the polymer is not ideal since in reality contact effects could be important in transferring force from the finger to the polymer layer. So, in this case ridge surface is represented by a segmented rigid body and the mechanical contact condition is formulated between each ridge-segment and the polymer.

From computational point of view, the last two models with contact interactions are nonlinear and are much more difficult to solve, particularly in this case when there are so many contact-based surfaces. It should be noted that due to multitude of contact formulations in the multi-NW models the solution process is relatively long and strongly depends on load magnitudes and Young's modulus of the polymer. The main challenge when performing these contact-based simulations is to find "universal" solver settings that would work for all the simulation cases of interest, e.g. for large range of applied load levels and values of polymer Young's modulus. Another computational complication is associated with each NW being connected to a separate external capacitor, which leads to a lot of electrical variables that have to be solved simultaneously. Fine-tuning of solver settings was performed and resulted in satisfactory solution convergence under wide range of simulation cases, which allowed to meet the objective of providing useful inputs for the PiezoMAT sensor design workflow, e.g. predicting design parameters of interest such as near-optimal values of Young's modulus and thickness of the encapsulating polymer as described below.

2.2.2 Initial numerical studies of the strain-induced electrical signals

Parametric numerical studies were performed in order to examine the differences between the three model alternatives in terms of generated strain-induced electrical outputs. Simulation results indicate the following (Figure 2.2.2.1):

- Contact-based interactions modify the deformation transfer process. "Mechanical cross-talk" appears to be intensified by introducing the contact effects into the system, which particularly evident when using a soft (e.g. PDMS) polymer.
- Model 3 predicts the lowest voltage output (ridge-polymer contact has the largest influence). Electrical outputs from loaded NWs predicted by Models 2 and 3 are ~20-30% and >80% lower, respectively (with respect to Model 1). For the unloaded NW4 the differences are >1000%.
- Model 1 predicts the lowest variability between voltages of the loaded NWs.

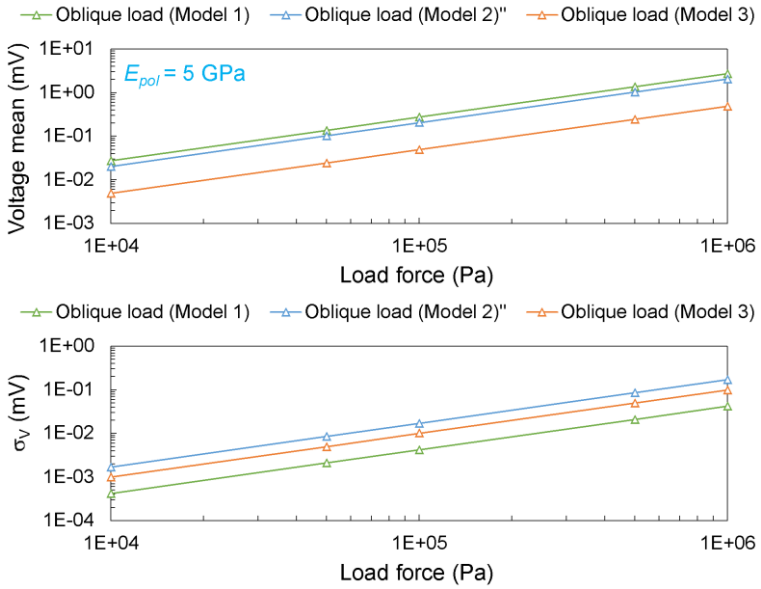

Figure 2.2.2.1: Plots of average voltage ($(V_{NW1}+V_{NW1}+V_{NW1})/3$) and standard deviation σ_V as a function of load force.

Numerical study was performed to determine a near-optimal (the most rational) value of polymer cap height h_{pol} (i.e. thickness of polymer layer above the NWs). Here, the term "near-optimal" implies the highest V_m accompanied by the lowest possible σ_V (since regions of maximum V_m and minimum σ_V do not coincide, we prioritize the former). 4 loading cases were examined in terms of force orientation: from pure vertical to strongly oblique. Simulation results indicate the following (Figure 3.6.3):

- Near-optimal polymer cap heights are within the range of $h_{pol} \approx 2 - 4$ μm for predominantly compressive loads, which are expected during PiezoMAT sensor usage.
- Variability of voltage signals generated by loaded NWs (σ_V) increases:
  - with larger horizontal force component. Model 2 predicts lower variability, particularly when horizontal force predominates over the vertical force.
  - with polymer cap height, particularly for larger horizontal force component. Nonlinearity of σ_V increase becomes stronger with increasing horizontal force component.

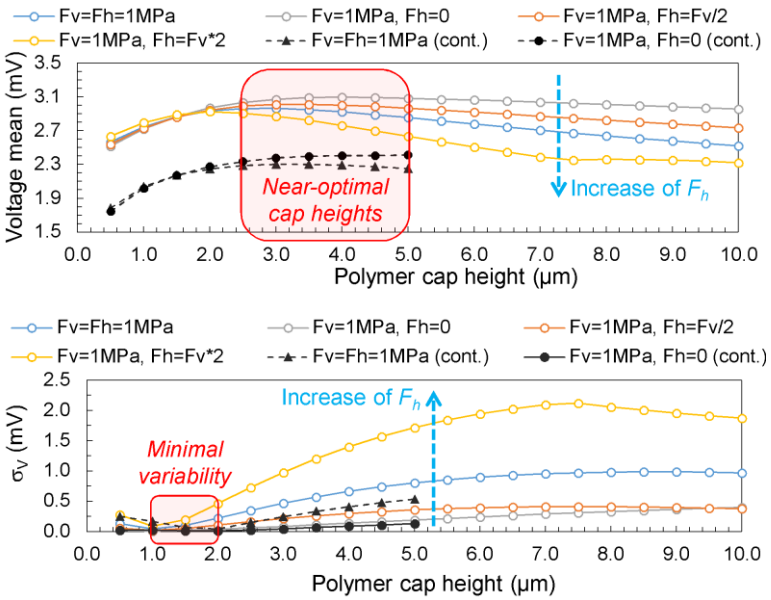

Figure 2.2.2.2: Plots of average voltage and standard deviation σ_V as a function of polymer cap height for different loading cases (using model alternatives 1 and 2 (cont.)).

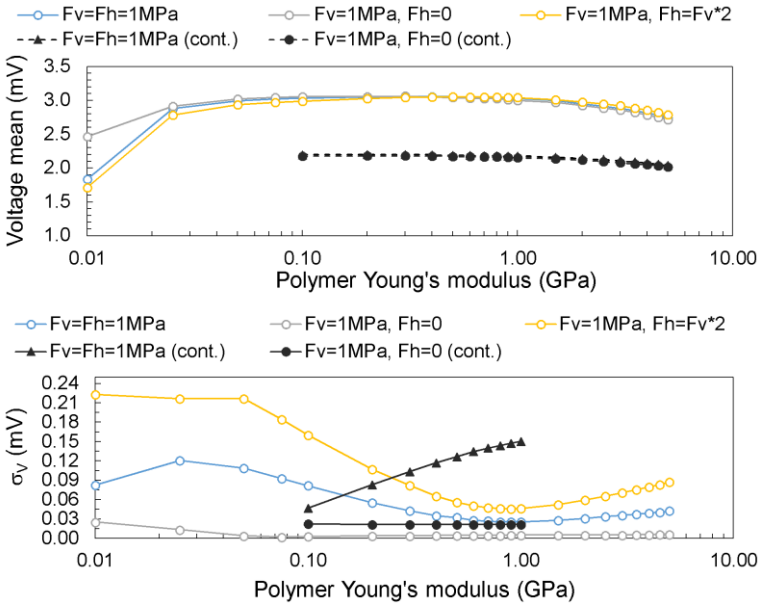

Figure 2.2.2.3: Plots of average voltage and standard deviation σ_V as a function of polymer Young's modulus for different loading cases (using model alternatives 1 and 2 (cont.)).

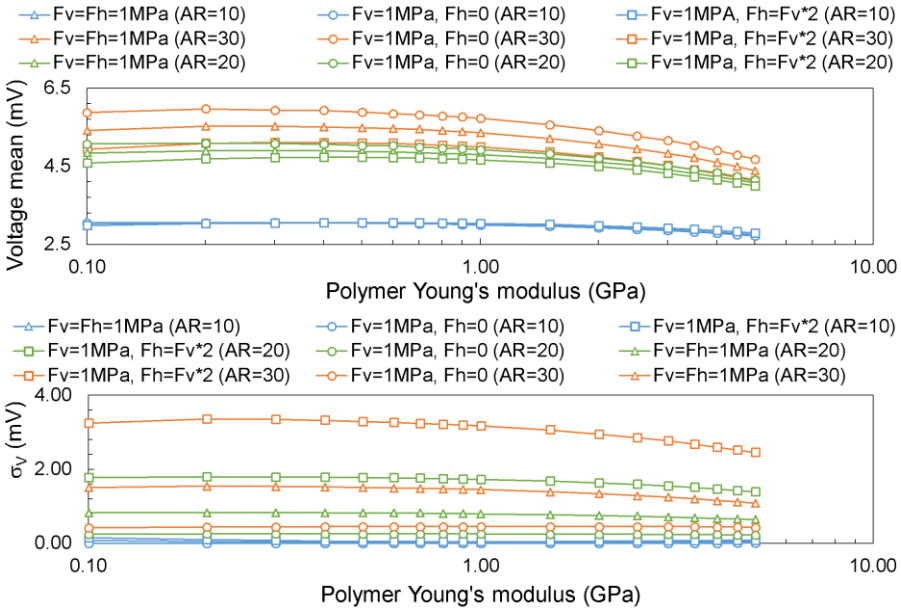

Figure 2.2.2.4: Plots of average voltage and standard deviation σ_V as a function of polymer Young's modulus for NW aspect ratios and different loading cases (using model alternative 1).

Numerical study was also performed to determine whether there is a near-optimal value of polymer Young's modulus in order to maximize average voltage output. In essence, the models predict that voltage output is not highly sensitive to E_{pol}, especially in the case of the contact-based model alternatives. Simulation results indicate the following:

- Insignificant change of average voltage for $E_{pol} \approx 0.2 – 2$ GPa (irrespective of NW aspect ratio, model version and load force orientation)(Figure 3.6.4).
- Near-optimal E_{pol} value is ~0.2 – 0.4 GPa (irrespective of NW aspect ratio and load force orientation). Increase in horizontal force component leads to very slight increase in near-optimal E_{pol} (Figure 3.6.4).
- Increase in aspect ratio of NWs:
  - As an advantage, leads to higher average voltage output for loaded NWs (6-fold increase in the ratio yields nearly 3-fold increase in V_m).

- As a downside, leads to pronounced increase in σ_V, i.e. variability of voltage signals generated by equally loaded NW1, NW2 and NW3 is magnified. The tendency is intensified with larger horizontal force component (Figure 2.2.2.4).
- As a downside, leads to pronounced increase in voltage generated by the unloaded NW4. The tendency is intensified with larger horizontal force component.

Comparing the relative significance of E_{pol} and h_{pol} as input parameters that are used for the rational design of the PiezoMAT sensor, it is concluded that it is more important to optimize h_{pol} since modification of E_{pol} above 0.2 GPa has insignificant influence on the values of both V_m and σ_V, particularly in the region of $E_{pol} \approx 0.2 – 2$ GPa.

2.2.3 Systematic numerical studies of the strain-induced electrical signals

The objective of the subsequent systematic numerical studies was to conduct a more extensive parameter space exploration using alternative 1 of model ver. FEM3.2 in order to check initial predictions (reported in Section 2.2.2) regarding near-optimal values of polymer cap height h_{pol} and polymer Young's modulus E_{pol}. The input parameters used for the study were as follows: polymer cap height h_{pol}, Young's modulus E_{pol}, ratio of horizontal force to vertical force F_h / F_v (ratio equal to zero implies that only vertical force is applied), aspect ratio of the nanowires ($AR_{NW} = h_{NW} / w_{NW}$).

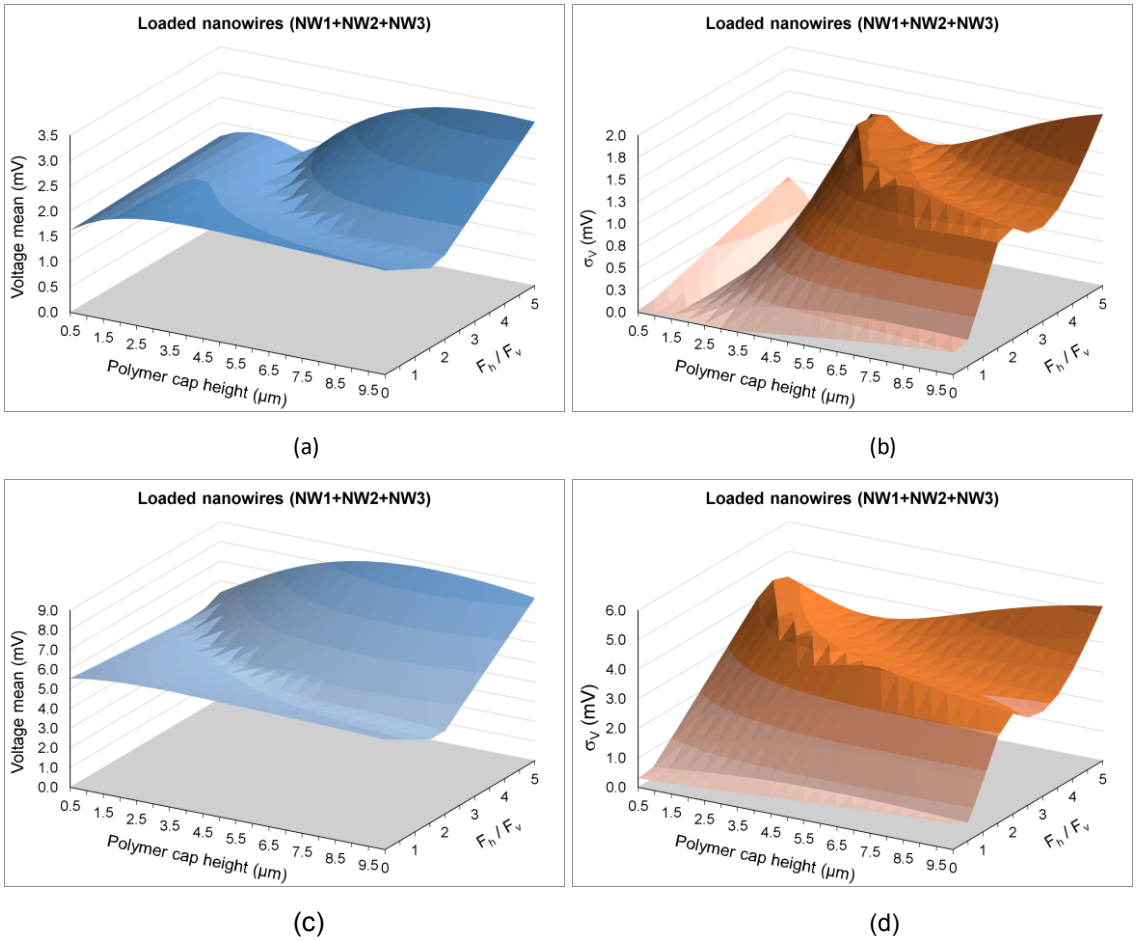

Figure 2.2.3.1: Voltage mean and standard deviation vs. polymer cap height and ratio of horizontal force to vertical force for NWs with aspect ratio of: 5 (a-b) and 30 (c-d). (E_{pol} = 0.5 GPa, F_v = 1 MPa).

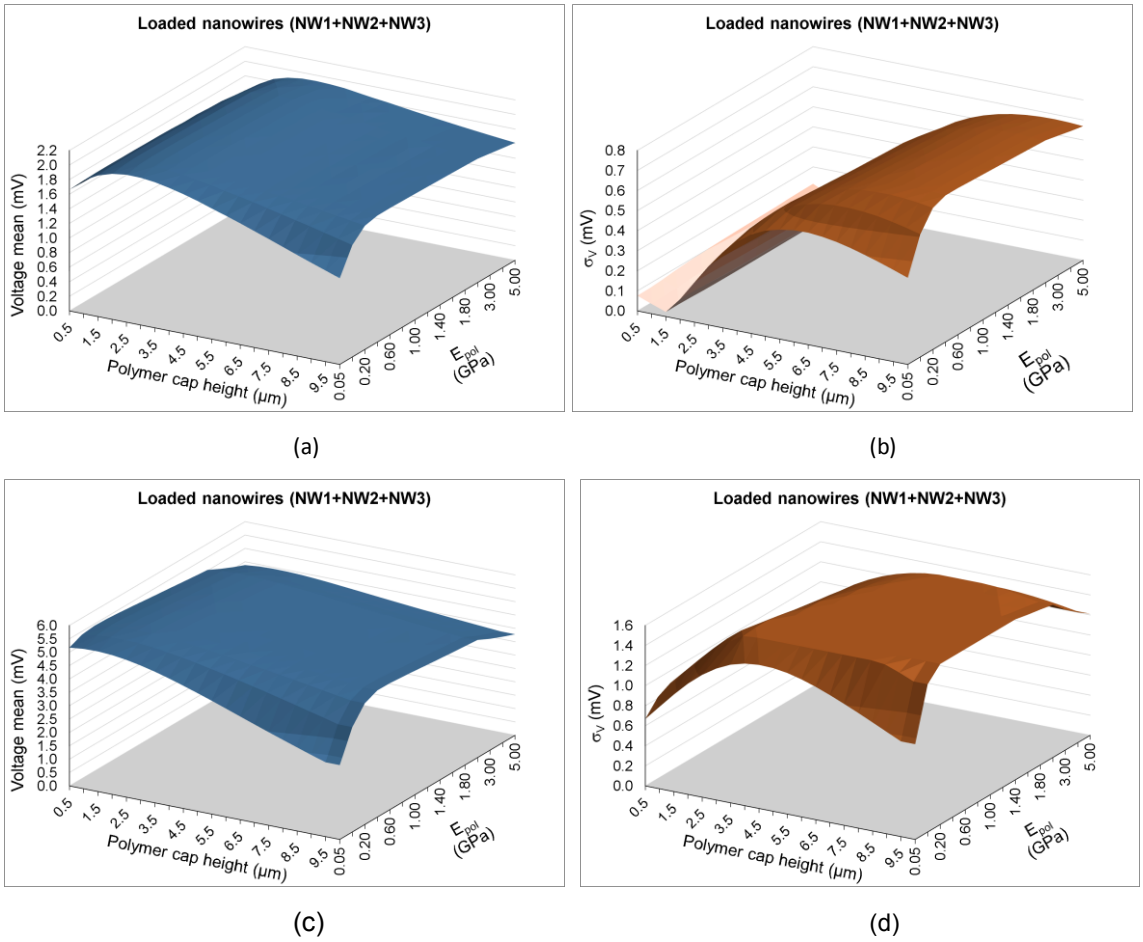

Figure 2.2.3.2: Voltage mean and standard deviation vs. polymer cap height and Young's modulus for NWs with aspect ratio of: 5 (a-b) and 30 (c-d). (F_v = F_h = 1 MPa).

Simulation data was used to construct 3D plots in Figures 2.2.3.1-2, which reveal variations of different complexity in terms of voltage mean V_m and standard deviation σ_V for different values of input parameters. Essentially, these results confirm the previous predictions of near-optimal values of E_{pol} and h_{pol}, though they provide additional insights on the interdependence of the parameters of interest. Simulation results indicate the following:

- Near-optimal E_{pol} value is **~0.2 – 0.5 GPa** (irrespective of NW aspect ratio and load force orientation). Increase in horizontal force component F_h leads to very slight increase in near-optimal $E_{pol.}$ Overall, values of V_m and σ_V are essentially insensitive to variation of polymer Young's modulus within a broad range of ~0.2 – 2 GPa (Figure 2.2.3.2).
- Near-optimal polymer cap heights for predominantly compressive loads (F_h / F_v = 0 – 1) are within the range of $\boldsymbol{h_{pol} \approx 2 – 4\ \mu m}$ for different aspect ratios (AR_{NW} = 5 – 30). Increase of AR_{NW} leads to very slight decrease of near-optimal h_{pol} (i.e. for AR_{NW} = 5, near-optimal $h_{pol} \approx 3 – 4$ μm; for AR_{NW} = 30, near-optimal $h_{pol} \approx 2 – 2.5$ μm).
- For predominantly compressive loads (F_h / $F_v \approx 0 – 1$) and for $E_{pol} \approx 0.2 – 2$ GPa:
  - As an advantage, V_m changes insignificantly with increasing h_{pol}. This favorable trend is valid both for low- and high-aspect ratio NWs (Figure 2.2.3.2a-c).
  - As a downside, σ_V changes more significantly with increasing h_{pol}. This unfavorable trend exhibits more pronounced and complex dependence on AR_{NW} (Figure 2.2.3.2b-d).
- Increase in aspect ratio of NWs:
  - As an advantage, leads to higher V_m (e.g. 6-fold increase in AR_{NW} yields nearly 3-fold increase in V_m).
  - As a downside, leads to pronounced increase in σ_V, i.e. variability of voltage signals generated by equally loaded NW1, NW2 and NW3 is magnified. The tendency is intensified with larger horizontal force component F_h (Figure 2.2.3.1b-d).

- Increase of h_{pol} and F_h introduces complex nonlinear variations of V_m and, particularly, σ_V (Figure 2.2.3.1). However, these unfavorable trends should not complicate the design and performance of the PiezoMAT sensor since near-optimal value of h_{pol} is relatively low and it is expected that vertical force component will predominate over the horizontal one (i.e. $F_h / F_v < 1$). Under the latter conditions variations of V_m and σ_V are essentially linear. Furthermore, Model 1 overestimates σ_V since inclusion of mechanical interfacial couplings (contact interactions) into the models tends to reduce σ_V (see Section 2.2.2).
- Comparing the relative significance of E_{pol} and h_{pol} as input parameters that are used for rational design of the PiezoMAT sensor, it is concluded that it is more important to optimize h_{pol} since modification of E_{pol} above 0.2 GPa has insignificant influence on the values of both V_m and σ_V, particularly in the region of $E_{pol} \approx 0.2 – 2$ GPa.

These results considered only the voltage outputs generated by the loaded NWs. However, initial prediction reported in Section 2.2.2 revealed that modification of the modeling assumptions (contact-based vs. no-contact mechanical coupling), geometric parameters, material properties and loading conditions has a marked effect on the electromechanical behavior of the unloaded NWs (NW4 and NW5). The associated interdependencies give rise to effects of mechanical crosstalk that have an impact on the generation of spurious signals, which are analyzed below.

2.2.4 Systematic numerical studies of the generated spurious electrical signals

In the conducted parametric study the same loading scenario was considered as previously, i.e. 3 NWs on the left are equally loaded ($F_1 = F_2 = F_3$), while the remaining 2 NWs on the right are not loaded. In the considered simulation case these unloaded NWs should ideally provide no electrical output, i.e. mechanical crosstalk (cross-coupling), influenced by proximity of adjacent NWs, should be minimized since these outputs constitute unwanted (spurious) signals that could degrade resolution and/or cause distortions of the fingerprint image. It should be noted that it is not fully clear whether the term “mechanical cross-talk (cross-coupling)” is strictly applicable for the considered case since NW4 & NW5 are not deformed because of the displacements of the NW1-NW3, though presence of NW1-NW3 certainly interferes with the force transfer process and, consequently, affects the deformation characteristics of the NW4 & NW5.

The objective of the systematic numerical studies was to conduct a more extensive parameter space exploration in order to examine electrical response of unloaded NWs (i.e. spurious signals) under different input parameters such as polymer cap height h_{pol}, Young’s modulus E_{pol}, aspect ratio of the nanowires ($AR_{NW} = h_{NW} / w_{NW}$), ratio of horizontal force to vertical force F_h / F_v (ratio of zero implies that only vertical force is applied). Simulation data was used to construct 3D plots in Figures 2.2.4.1-2, which show variations of spurious voltage signals V_{NW4} and V_{NW5} for different values of input parameters. For comparison purposes Table 1 summarizes values of average ratios (percentages) of NW4 & NW5 voltage outputs to voltage means for loaded NWs ($V_m = (V_{NW1} + V_{NW2} + V_{NW3})/3$) for different combinations of input parameters.

Table 2.2.4.1: Comparison of magnitudes of electrical outputs of unloaded NWs with respect to voltage mean for loaded NWs.

No.	*Combinations of input parameters*	*Average percentage for NW4 ($(V_{NW4} / V_m) \times 100$), %*		*Average percentage for NW5 ($(V_{NW5} / V_m) \times 100$), %*	
		$AR_{NW} = 5$	$AR_{NW} = 30$	$AR_{NW} = 5$	$AR_{NW} = 30$
1.	$F_h / F_v = 0 – 1$; $h_{pol} = 2 – 4$ μm	5.34	23.14	0.45	1.79
2.	$F_h / F_v = 2 – 5$; $h_{pol} = 5 – 10$ μm	97.12	108.84	26.99	31.40
3.	$E_{pol} = 0.2 – 0.4$ GPa; $h_{pol} = 2 – 4$ μm	9.46	34.87	0.91	1.65
4.	$E_{pol} = 1 – 5$ GPa; $h_{pol} = 5 – 10$ μm	47.61	58.33	9.84	10.59

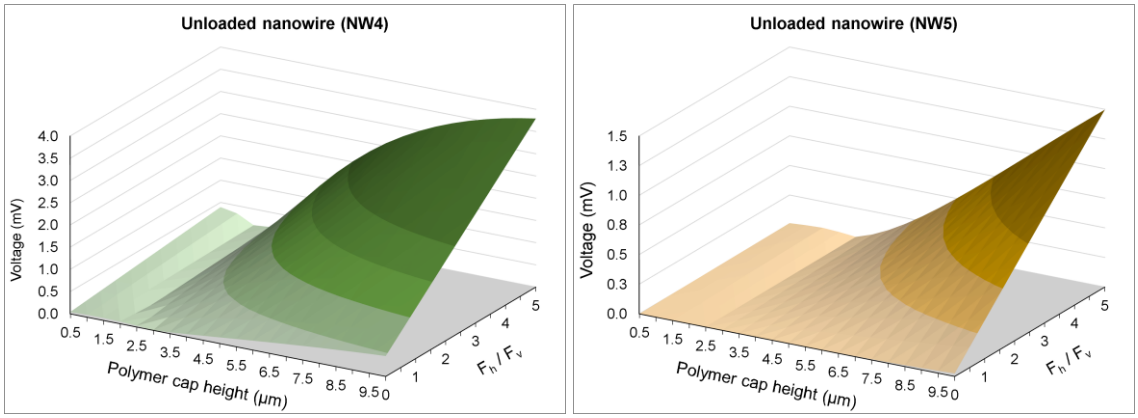

(a) (b)

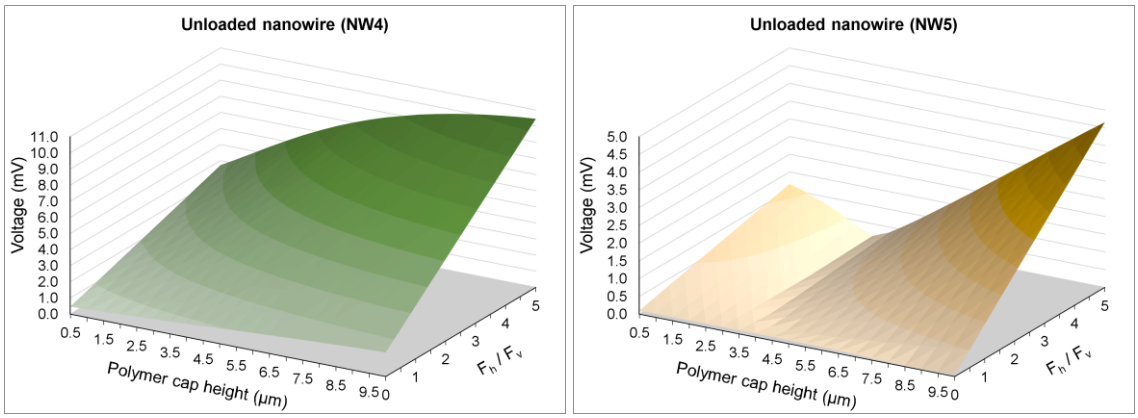

(c) (d)

Figure 2.2.4.1: Voltage output of the unloaded NWs vs. polymer cap height and ratio of horizontal force to vertical force for NWs with aspect ratio of: 5 (a-b) and 30 (c-d). (E_{pol} = 0.5 GPa, F_v = 1 MPa).

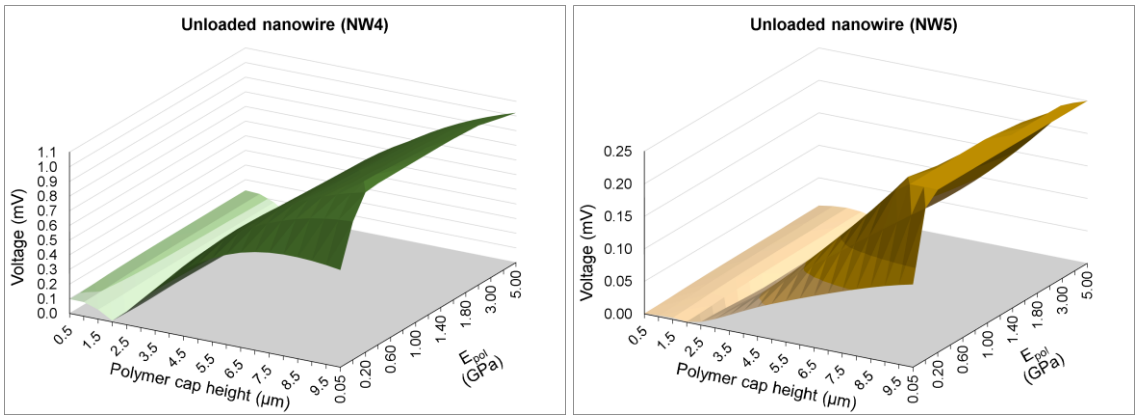

(a) (b)

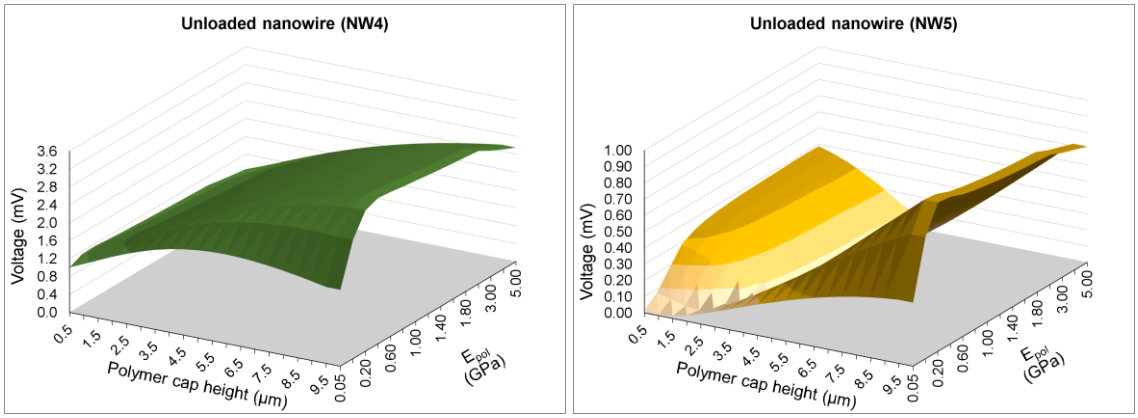

(c) (d)

Figure 2.2.4.2: Voltage output of the unloaded NWs vs. polymer cap height and Young's modulus for NWs with aspect ratio of: 5 (a-b) and 30 (c-d). (F_v = F_h = 1 MPa).

Simulation results indicate the following:

- Increase in F_h / F_v has the following effects (Figure 2.2.4.1):
  - For higher h_{pol} values the general tendency is the amplification of spurious signals: large h_{pol} in conjunction with large F_h / F_v leads to pronounced increase of spurious voltage outputs (e.g. output from NW4 may even exceed average voltage of the loaded NWs, see No. 2 in Table 2.2.4.1).
  - For predominantly compressive loads (F_h / F_v = 0 – 1) the spurious voltage outputs are (see No. 1 in Table 2.2.4.1): i) minimized for NW4, but are still significant, particularly for AR_{NW} = 30; ii) extremely small for NW5 in the case of near-optimal h_{pol} values (2 – 4 μm) both for small and large NW aspect ratios, constituting only ~0.5 – 2% of the average signal V_m of loaded NWs.
  - For near-optimal h_{pol} values and AR_{NW} = 5 the outputs are essentially insensitive to increasing F_h, which is not the case for AR_{NW} = 30.
- Increase in E_{pol} has the following effects (Figure 2.2.4.2):
  - For higher h_{pol} values the general tendency is the rapid increase of voltage outputs only in the region of E_{pol} = 0.05 – 0.6 GPa (outputs are stabilized further on). Large h_{pol} in conjunction with large E_{pol} leads to pronounced amplification of the spurious signals (see No. 4 in Table 2.2.4.1).
  - In the region corresponding to near-optimal values of E_{pol} and h_{pol} (i.e. ~0.2 – 0.4 GPa and 2 – 4 μm, respectively) the spurious voltage outputs are (see No. 3 in Table 1): i) minimized for NW4, but are still significant, particularly for AR_{NW} = 30; ii) extremely small for NW5 both in the case of small and large NW aspect ratios, constituting only ~1 – 2% of the average signal V_m of loaded NWs.

Reported numerical results demonstrate that variation of geometric parameters, material properties and loading conditions has a marked effect on the electromechanical behavior of unloaded NWs through complex deformation transfer process in the considered heterogeneous medium. The associated interdependencies give rise to parasitic effects related to mechanical coupling. Key conclusions are that:

- As major advantage: voltage outputs from unloaded NWs are significantly reduced (attain near-minimal magnitudes) when using near-optimal values of E_{pol} and h_{pol}. In this case the impact of parasitic mechanical crosstalk is rapidly attenuated and the spurious signals of NW5 become considerably smaller in comparison to the preceding NW4.
- As a downside: mechanical crosstalk is amplified when increasing AR_{NW}, h_{pol} and F_h. Rate of attenuation of the mechanical crosstalk tends to diminish with increasing h_{pol}, which suggests that in the case of thicker encapsulation layer a larger number of successive unloaded NWs would generate appreciable spurious signals.

2.2.5 Implementation of the piezoelectric chip-based model ver. FEM3.2

Numerical studies with the different alternatives of the structurally-idealized FE model ver. FEM3.2 (i.e. excluding multi-layer chip stack) were described in Sections 2.2.2-2.2.4. Subsequently, the structurally-idealized model ver. FEM3.2 was made more realistic, i.e. upgraded to the "chip-based" configuration by including the associated stack layers (Figure 2.2.5.1) in accordance with the approved PoC3 chip layouts (D4.1). The new model includes two polymeric layers (dielectric and conducting) and takes into account the dielectric properties of all the chip components. Effects of semiconductor physics were excluded in this model, but were further incorporated into model ver. FEM3.4. Separate numerical studies were not performed with the chip-based model ver. FEM3.2 since its implementation was an intermediate step in developing the final and the most complex model ver. FEM3.4, which is the most accurate both physically and structurally, and was used for the comparisons with experimental results and explanation of the measured electrical signals (see below).

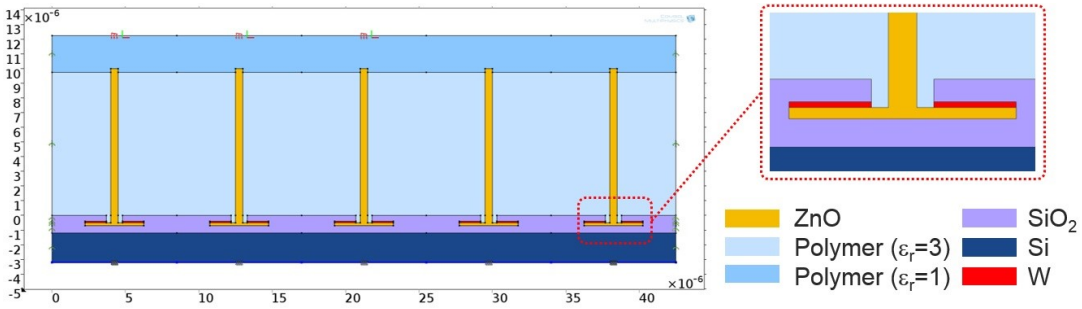

Figure 2.2.5.1: Piezoelectric chip-based model (ver. FEM3.2) of a periodic array of the individually-addressable ZnO nanowire-based Option 3 piezo-pixels, which are integrated onto a multi-layer chip stack and encapsulated within the dielectric and conducting PMMA-based polymeric layers (ZnO – piezoelectric/dielectric.). Piezo-pixel properties: w_{NW} = 500 nm, h_{NW} = 5 – 15 µm, C_{ext} = 10 fF.

2.3 Piezo-semiconductive chip-based model of the encapsulated Option 3 ZnO NW array (ver. FEM3.4)

2.3.1 Model implementation

It should be reminded that characterization results of PoC3 were initially compared to the structurally-idealized single-NW piezo-semiconductive model (ver. FEM3.3). Though only approximate comparisons could be performed, it was determined that the predicted strain-induced current signal is by several orders of magnitude lower in comparison to the measured one. Such significant mismatch between the numerical and experimental results could not be explained by the different sources of error such as: variability of N_{D0} and Schottky barrier height (e.g. from batch to batch), variability of number of NWs per pixel and the orientation of NWs (vertical alignment is assumed in simulations), modeling idealizations (e.g. replacing NW bundle with a single NW having the same dimensions as the bundle). Therefore, it was concluded that some other principles of charge generation could participate in the mechanical-to-electrical energy conversion within the ZnO NWs. State of the art review (link) was performed to analyze recent findings about the electro-mechanical behavior of the strain-responsive piezoelectric-semiconductive nanotransducers. The review revealed that this is still a very hot topic in the scientific community with many unanswered questions, which are concerned with the fundamental underlying mechanism of mechanical-to-electrical conversion within the strain-responsive piezoelectric-semiconductive devices, particularly in the case of Schottky-contacted ones. Based on the results of the review, it was concluded that the obtained several-orders-of-magnitude discrepancies between the results of PoC3 simulations and characterizations could not be eliminated if the developed piezo-semiconductive model ver. FEM3.3 was complemented with other effects mentioned in the review (e.g. pyroelectricity or second-order piezoelectricity).

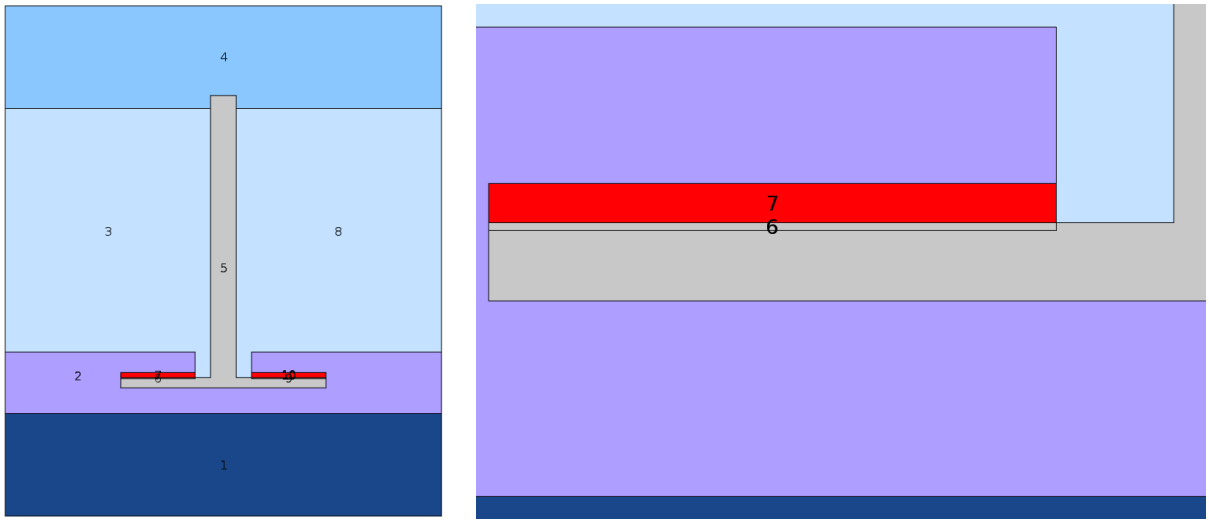

(a) (b)

Figure 2.3.1: (a) Piezo-semiconductive chip-based model (ver. FEM3.4) of the encapsulated Option 3 ZnO NW, which is integrated onto a multi-layer chip stack and encapsulated within the dielectric and conducting PMMA-based polymeric layers (ZnO – piezoelectric/semiconducting, NW properties: w_{NW} = 500 nm, h_{NW} = 5 µm, C_{tot} = 10 fF). (b) Close-up view of the left side of seed layer (6 – depletion region, 7 – Tungsten electrode).

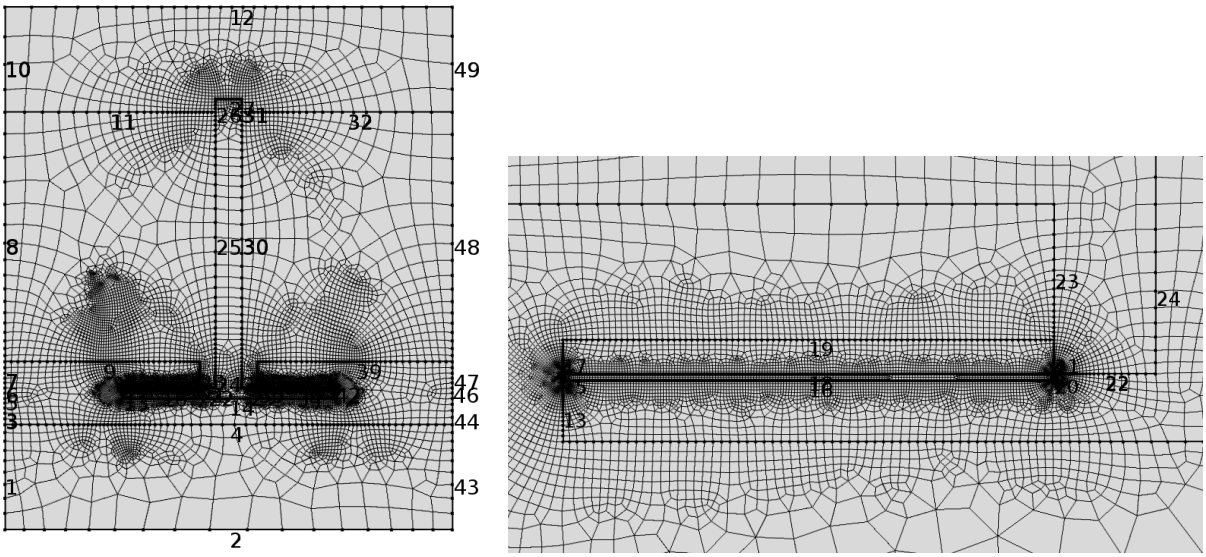

(a) (b)

Figure 2.3.2: (a) COMSOL model ver. FEM3.4 meshed with quadrilateral elements (~300k DOFs). (b) Close-up view of the seed layer with very finely meshed depletion region and its surroundings.

Therefore, the decision was made to dedicate efforts to integrate the previously developed FE models ver. FEM3.3 and the chip-based ver. FEM3.2 into a single most comprehensive model having the most realistic structural, physical and electrical configuration so as to match the DEMO3 configuration as close as possible. For making comparisons with the PoC3/FEMO3 characterization results it was sufficient to model and analyze just a single cell of the NW array (Figure 2.3.1). The model is adaptive and can be easily extended to the multi-NW configuration if array-related phenomena had to be analyzed (as in the case of models ver. FEM3.2). The most significant challenge in simulations performed with the model ver. FEM3.4 is related to the high number of DOFs involved (~300k for a single cell) due to necessity to finely mesh the depletion regions at Schottky contacts (Figure 2.3.2).

2.3.2 Results of numerical studies and experimental verification

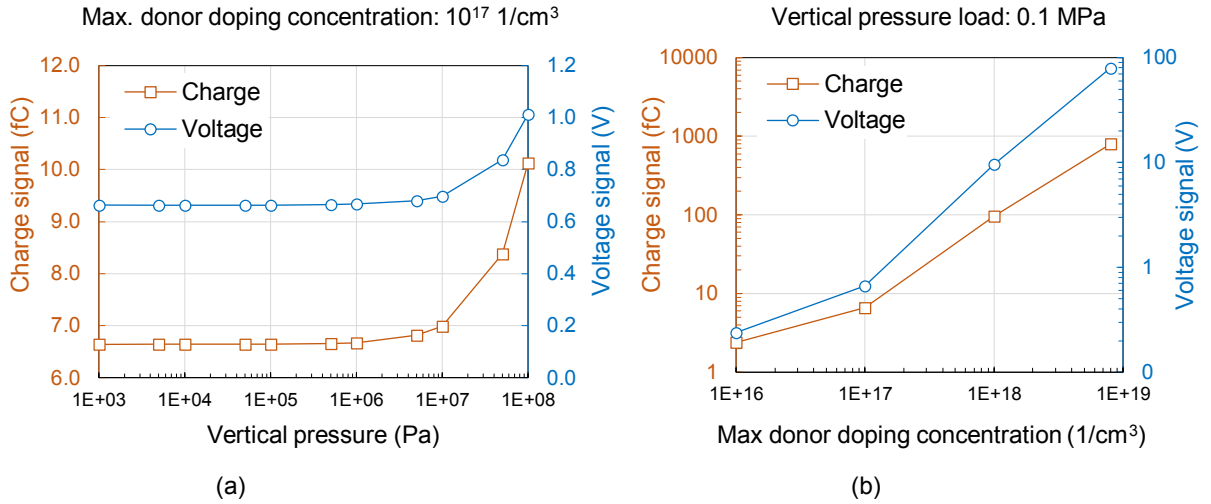

Figure 2.3.2.1: Representative numerical results obtained with the piezo-semiconductive chip-based model (ver. FEM3.4) of the encapsulated Option 3 ZnO NW (with Schottky and ohmic contacts at the bottom and top electrodes, respectively). The plots show variation of electrical signals as a function of vertical pressure (a) and maximum donor doping concentration in ZnO (b). Model properties: NW width – 2 μm, NW length – 3.5 μm, external capacitor connected to NW – 10 fF.

Conducted numerical studies indicate the following:

- Magnitude of electrical signals strongly depends on the maximum donor doping (n-type) concentration in ZnO (Figure 2.3.2.1): the most pronounced increase is predicted for 10^{18} – 10^{19} 1/cm^3. The predicted charge signal at 10^{18} 1/cm^3 is on the order of 100 fC, which is in agreement with the signal levels measured on DEMO3.
- The predicted trends of variation of electrical signals with the increasing pressure load (Figure 2.3.2.1) implies that two operation modes could be distinguished with respect to the magnitude of applied load (for pixel diameters of several micrometers!):
  a) In low-load range (roughly: <1 MPa) the sensor operates in *force-activated regime*, which essentially corresponds to the binary sensing mode. In this load range the generated total electrical signal has relatively high magnitude that cannot be attributed to the strain-induced piezoelectric effect and is essentially insensitive to the increasing compression load. To be more specific, the strain-induced sensitivity is the same throughout the low- and high-load ranges, but in low-load range the magnitude of the strain-induced electrical signal is extremely small in comparison to the total electrical signal that is generated by the NW. Force-dependent signals in the low-load range could be potentially attained by: i) (significantly) increasing pixel area to obtain parallel-connection of the NWs, thereby enabling increase of the charge and current outputs), ii) series-connection of the pixels, thereby enabling increase of the voltage.
  b) In high-load range (roughly: >1-2 MPa) the sensor operates in *force-dependent regime* since the electrical signals become sensitive to the increasing load (force-dependency is considerably stronger in comparison to the Option 2 model ver. FEM2.3). Analogously to the low-load case, the predicted relatively high electrical outputs cannot be explained by the piezo-effect alone.
  c) The predicted relatively high electrical signals generated by the modeled Schottky-contacted piezo-semiconductor/metal sandwich microstructure suggest that the strain-induced piezo-charges might not be the primary factor contributing to the mechanical-to-electrical energy conversion process. State of the art review reveals that the fundamental underlying mechanism of this process is not yet fully understood in terms of the piezotronic effect [1]. Some of the best

[1] W. Wu and Z.L. Wang. Piezotronics and piezo-phototronics for adaptive electronics and optoelectronics. Nature Reviews Materials, vol. 1(7), 2016, 16031.

candidate explanations include strain-dependent modification of the Schottky barrier height, increased electron density and reduced resistance in ZnO under compression [2,3].

- The predicted strain-induced sensitivities are: for voltage – 3.5 μV/kPa, for charge – 3.5×10^{-5} fC/kPa, for current – 7.8×10^{-4} fA/kPa. Strain-induced voltage sensitivity is very close to the experimental values reported in the literature for the hydrothermally-grown ZnO NW arrays: ~1 – 5 μV/kPa for the tactile pressure sensor [4] (pixel size: 500 μm × 500 μm) and ~8 μV/kPa for the large-area nanogenerator [5] (pixel size: ~4 mm^2). It should be noted that force-dependent electrical signals are indeed reported for the tactile pressure sensor in the low-load range of 10 – 200 kPa, but the area of the pixel in this case is about 8×10^4 times(!) larger in comparison to the DEMO3 case.
- Interestingly, the predicted strain-induced current density reaches about 25 nA/cm^2 (at 1 MPa), which is comparable to the experimental values of 6 – 9 nA/cm^2 reported for the aforementioned large-area nanogenerator (at 1.25 – 6.25 MPa). The predicted higher value in this case can be explained by the fact that in the FE model the pixel area is fully occupied by a single ZnO NW (i.e. NW fill ratio is 100%), meanwhile in the case of the nanogenerator the pixel is sparsely populated with the NWs.
- Good agreement between the simulated values and the experimental values (obtained both within the PiezoMAT consortium and by other research groups) demonstrates that the predictions of the model are credible.

2.4 Summary

Main results of the numerical studies for Option 3 NW array are as follows:

- Using the multi-NW piezoelectric model of the encapsulated Option 3 ZnO NW array (ver. FEM3.2):
  - Near-optimal values of the encapsulating polymer Young's modulus were predicted to be in the range of about 0.2 – 0.5 GPa (irrespective of NW aspect ratio and pressure load orientation). The recommended near-optimal values of polymer cap height are in the range of about 2 – 4 μm (irrespective of NW aspect ratio for the predominantly compressive loads). At these near-optimal values, the useful piezoelectric signals are maximized and the parasitic (spurious) signals – minimized.
  - Compared to Option 2, NW array of Option 3 exhibits less complex and more favorable electromechanical behavior when subjected to varying input parameters (e.g. NW aspect ratios, load orientations). For example, spurious signals in this case are considerably lower, which implies higher native spatial resolution in comparison to the analogous implementation of Option 2 fingerprint sensor.
- Using the piezo-semiconductive chip-based model of the encapsulated Option 3 ZnO NW array (ver. FEM3.4) with Schottky and ohmic contacts at the bottom and top electrodes, respectively (ZnO NW pixel size is 3.5 μm × 2 μm):
  - The predicted trends of variation of electrical signals with the increasing pressure load implies that two operation modes could be distinguished with respect to the magnitude of applied load (for pixel diameters of several micrometers!):
    a) In low-load range (roughly: <1 MPa) the sensor operates in *force-activated regime*, which essentially corresponds to the binary sensing mode. In this load range the electrical signals have relatively high magnitude that cannot be attributed to the strain-induced piezoelectric effect and are insensitive to the increasing compression load. Force-dependent signals in the low-load range could be potentially attained by: i) (significantly) increasing pixel area to obtain parallel-connection of the NWs, thereby enabling increase of the charge/current outputs), ii) series-connection of the pixels, thereby enabling increase of the voltage output.

[2] P. Keil, T. Froemling, A. Klein, et al. Piezotronic effect at Schottky barrier of a metal-ZnO single crystal interface. Journal of Applied Physics, vol. 121(15), 155701, 2017.
[3] R. Baraki, N. Novak, M. Hofstaetter, et al. Varistor piezotronics: Mechanically tuned conductivity in varistors. Journal of Applied Physics, vol. 118(8), 085703, 2015.
[4] B.P. Nabar, Z. Celik-Butler, D.P. Butler. Self-Powered Tactile Pressure Sensors Using Ordered Crystalline ZnO Nanorods on Flexible Substrates Toward Robotic Skin and Garments. IEEE Sensors Journal, vol. 15(1), p. 63-70, 2014.
[5] S. Xu, Y. Qin, C. Xu, et al. Self-powered nanowire devices. Nature Nanotechnology, vol. 5(5), p. 366-373, 2010.

b) In high-load range (roughly: >1-2 MPa) the sensor operates in *force-dependent regime* since the electrical signals become sensitive to the increasing load (force-dependency is considerably stronger in comparison to the Option 2 model ver. FEM2.3). Analogously to the low-load case, the predicted relatively high electrical outputs cannot be attributed to the piezoelectric effect alone.

c) The predicted relatively high electrical signals generated by the modeled Schottky-contacted piezo-semiconductor/metal sandwich microstructure suggest that the strain-induced piezo-charges might not be the primary factor contributing to the mechanical-to-electrical energy conversion process. State of the art review reveals that the fundamental underlying mechanism of this process is not yet fully understood in terms of the piezotronic effect. Some of the best candidate explanations include strain-dependent modification of potential barrier height of the Schottky contact, increased electron density and reduced resistance in ZnO under compression.

- The values of the predicted strain-induced voltage sensitivity and strain-induced current density are in good agreement with the experimental values reported for the analogous pressure sensors based on ZnO NWs.
- Magnitude of electrical signals strongly depends on the maximum donor doping (n-type) concentration in ZnO: the most pronounced increase is predicted for 10^{18} – 10^{19} 1/cm^3. The predicted charge signal at 10^{18} 1/cm^3 is on the order of 100 fC, which is in agreement with the signal levels measured on DEMO3.
- Good agreement between the simulated values and the experimental values (obtained within the PiezoMAT consortium and by other research groups) demonstrates that the predictions of the most realistic piezo-semiconductive model ver. FEM3.4 are credible.

3 Multiphysics finite element modeling of the bottom-bottom contacted ZnO nanowires for bending force sensing (Option 2)

3.1 Overview of the implemented models (Option 2)

A wide range of multiphysics FE models of Option 2 arrayed vertical ZnO NWs were implemented by KTU using COMSOL Multiphysics® software (Table 3.1.1). Analogously to the case of Option 3, the NWs were modeled as individually-addressable pressure sensing pixels by connecting them to separate external capacitors, which represented the readout circuitry of the sensor. Modeling and simulation results for model versions FEM2.1 were reported in D3.3. Meanwhile, D3.4 focuses on the results obtained with the model versions FEM2.2 and FEM2.3.

Table 3.1.1: Summary of the implemented FE models (Option 2).

Version No.	***Type of model***	***Main features***	***Model images***
FEM2.1	*Single-NW piezoelectric model (3D)*	▪ Idealized structural & electrical configuration (classical piezoelectric theory): - ZnO: dielectric. - Electrical contacts: ohmic. - Electrical properties of all dielectric and conducting stack layers accounted for. ▪ No encapsulation.	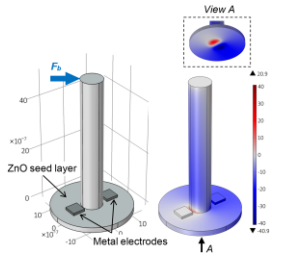
FEM2.2	*Encapsulated multi-NW piezoelectric chip-based model (2D)*	▪ Realistic structural configuration: NWs integrated on a multi-layer chip stack & encapsulated in a polymer. ▪ Idealized electrical & physical configuration: - ZnO: dielectric. - Electrical contacts: ohmic. - Electrical properties of all dielectric and conducting stack layers accounted for.	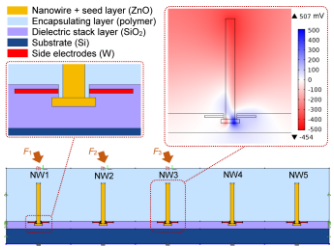
FEM2.3	*Encapsulated single-NW piezo-semiconductive chip-based model (2D)* /directly extendable to NW array/	▪ Realistic structural configuration: NWs integrated on a multi-layer chip stack and encapsulated in a polymer. ▪ Realistic electrical & physical configuration: - Coupled piezoelectric & semiconducting properties in ZnO. - Electrical contacts: ohmic or Schottky (nonlinear) - Electrical properties of all stack layers accounted for.	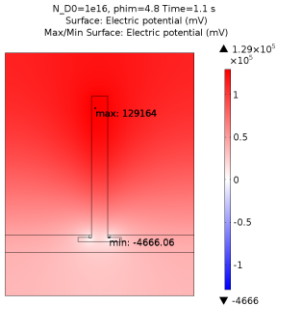

3.2 Multi-NW piezoelectric chip-based model of the encapsulated Option 2 ZnO NW array (ver. FEM2.2)

3.2.1 Model implementation

The multi-NW piezoelectric chip-based model of the encapsulated Option 2 ZnO NW array was implemented by including the associated stack layers (Figure 3.2.1.1) in accordance with the approved PoC2 chip layouts (D4.1). Analogously to the piezoelectric chip-based model of Option 3 NW array (ver. FEM3.2), this model also takes into account the dielectric properties of all the chip components. The piezo-pixel is configured so as to collect charges through tungsten side electrodes, which may be either

separated from ZnO (as in Figure 3.2.1.1) or they may be contacting ZnO (as in the case of model FEM2.3 that closely resembles the configuration of PoC2 developed by MTA).

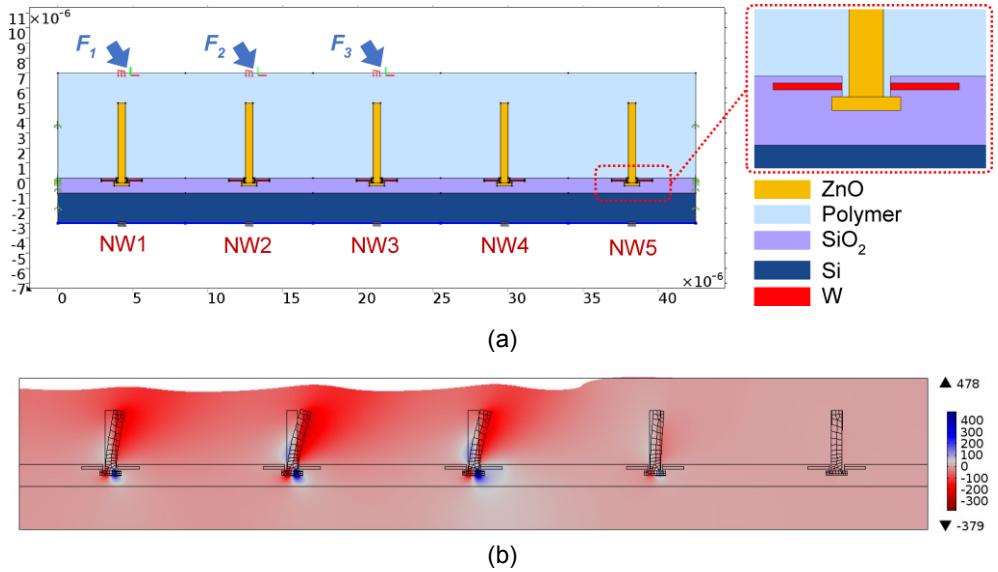

Figure 3.2.1.1: (a) Piezoelectric chip-based model (ver. FEM2.2) of a periodic array of the individually-addressable ZnO nanowire-based Option 2 piezo-pixels. Piezo-pixel properties: w_{NW} = 500 nm, h_{NW} = 5 – 15 µm, inter-NW gap d_{NW} = 8 µm, C_{ext} = 10 fF. (b) Visualization of electric potential distribution (side bar – in mV) in the deformed NW array, which was obliquely loaded with pressure load $F_h = F_v$ = 1 MPa.

3.2.2 *Systematic numerical studies of the strain-induced electrical signals*

As previously, systematic numerical studies were conducted by subjecting the top of the PMMA-based encapsulation layer with a downward ramping load that imitates pressing with a fingertip. It is assumed that the array is loaded by a fingertip region corresponding to a ridge edge, i.e. the ridge presses NW1, NW2 and NW3, while the remaining NW4 and NW5 are not loaded. Outputs of these unloaded NWs are considered to be spurious signals that would degrade sensor resolution. Therefore, as previously reported, the design targets are (for the case of equal load $F_1 = F_2 = F_3$): i) to maximize mean voltage ($V_m = (V_{NW1} + V_{NW2} + V_{NW3})/3$) and minimize variability (σ_V); ii) to minimize spurious signals (V_{NW4}, V_{NW5}).

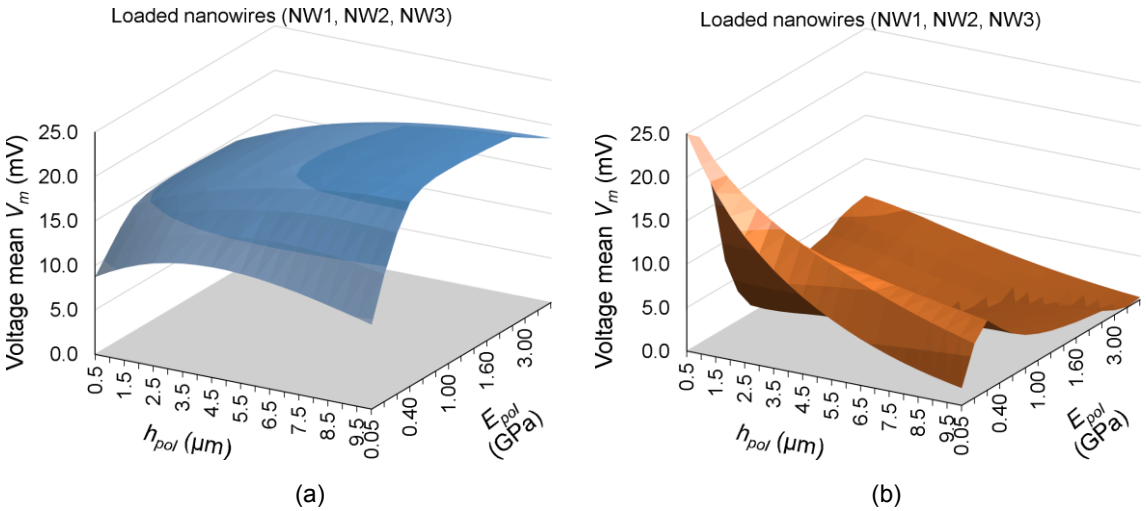

Figure 3.2.2.1: Surface plots of average voltage output generated by the directly loaded piezo-pixels as a function of polymer cap height and Young's modulus for the case of: (a) pure vertical load of F_v = 1 MPa, (b) oblique load of $F_h = F_v$ = 1 MPa (w_{NW} = 0.5 µm, h_{NW} = 15 µm).

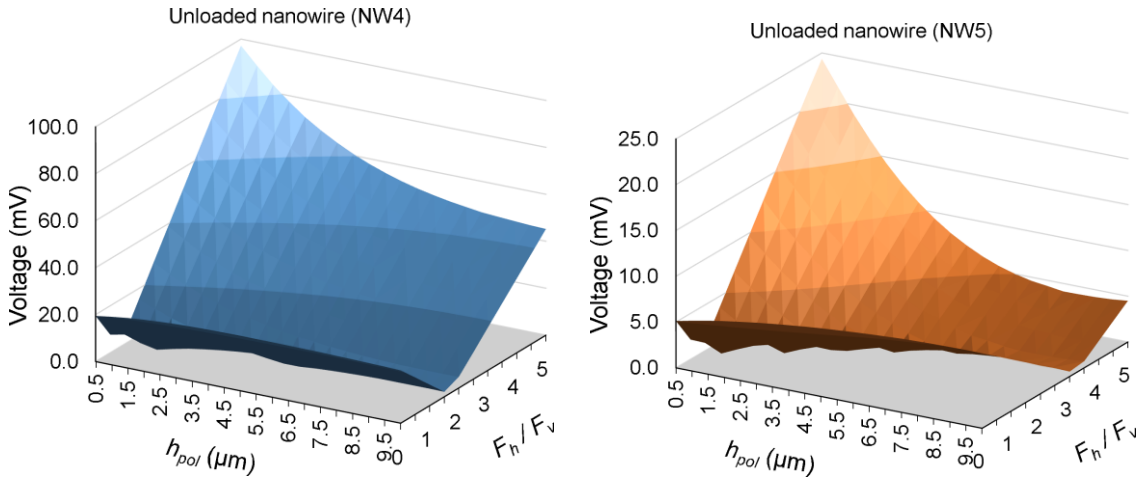

(a) (b)

Figure 3.2.2.2: Surface plots of spurious signals generated by the unloaded piezo-pixels as a function of polymer cap height and horizontal-to-vertical force ratio (F_V = 1 MPa, w_{NW} = 0.5 μm, h_{NW} = 15 μm, E_{pol} = 0.5 GPa).

Parametric study was performed to predict the most rational (near-optimal) values of polymer Young's modulus E_{pol} and cap height h_{pol} by constructing 3D plots for low and high aspect ratio NWs when the array was deformed by pressure load of varying orientation (e.g. Figure 3.2.1.1). Here, the term *near-optimal* implies the highest V_m accompanied by the lowest possible standard deviation σ_V. Figure 3.2.2.1 reveals strong dependence of V_m on load orientation, exhibiting complex variation of V_m with changing E_{pol} and h_{pol} when horizontal load component is introduced. Numerical results also indicate the spurious voltage signals to be high (Figure 3.2.2.2) with respect to the useful signals generated by NW1, NW2 and NW3 (even under pure compression). Impact of mechanical crosstalk is more significant for Option 2, i.e. spurious signals are significantly larger when compared to Option 3. Simulations reveal that near-optimal values strongly depend on the load orientation. The recommendation for the near-optimal values is based on the realistic assumption that there will be at least some horizontal load component during the actual sensor usage. Therefore, the recommended near-optimal cap height would be the same as for Option 3 (2-4 μm), while softer polymer would be more suitable for Option 2 (ca. $E_{pol} \approx 0.2$ GPa).

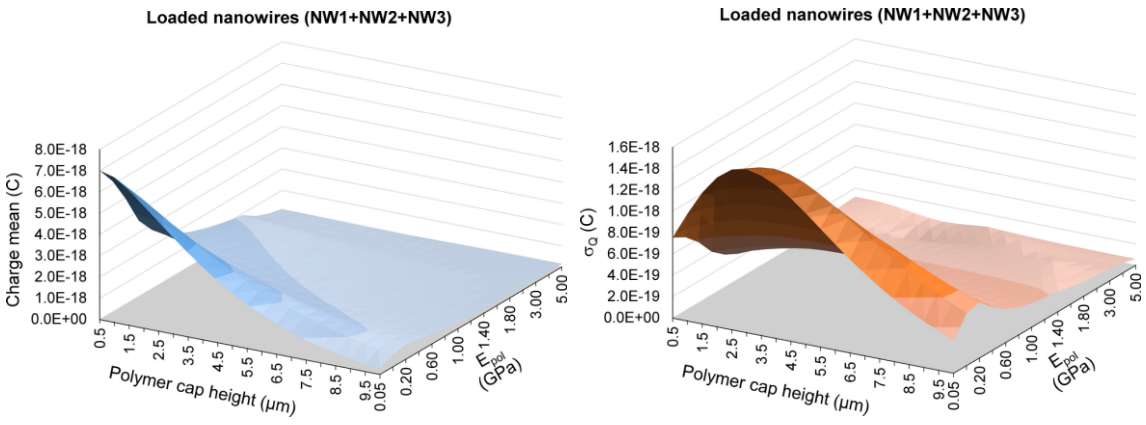

(a) (b)

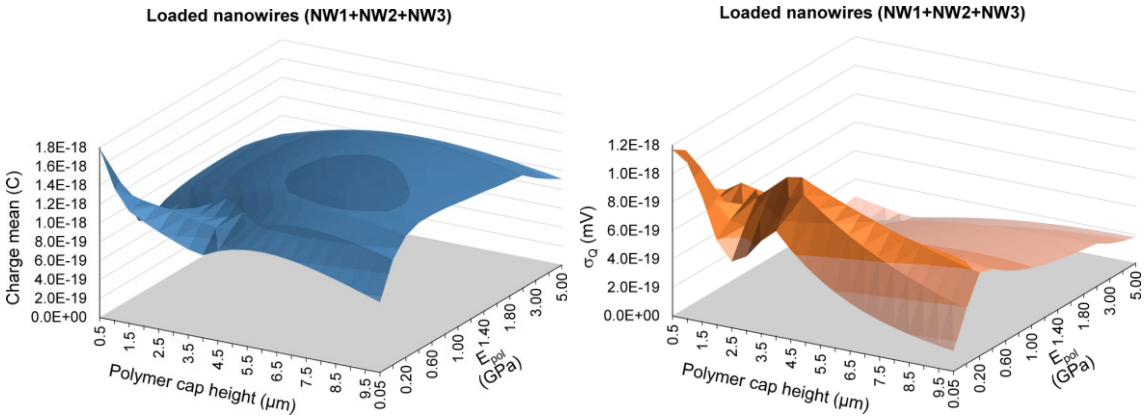

(c) (d)

Figure 3.2.2.3: Surface plots of the average charge outputs and their variability as a function of polymer cap height and Young's modulus for the case of oblique load $F_h = F_v = 1$ MPa for: (a)-(b) $AR_{NW} = 5$ ($w_{NW} = 0.5$ μm, $h_{NW} = 2.5$ μm); (c)-(d) $AR_{NW} = 30$ ($w_{NW} = 0.5$ μm, $h_{NW} = 15$ μm).

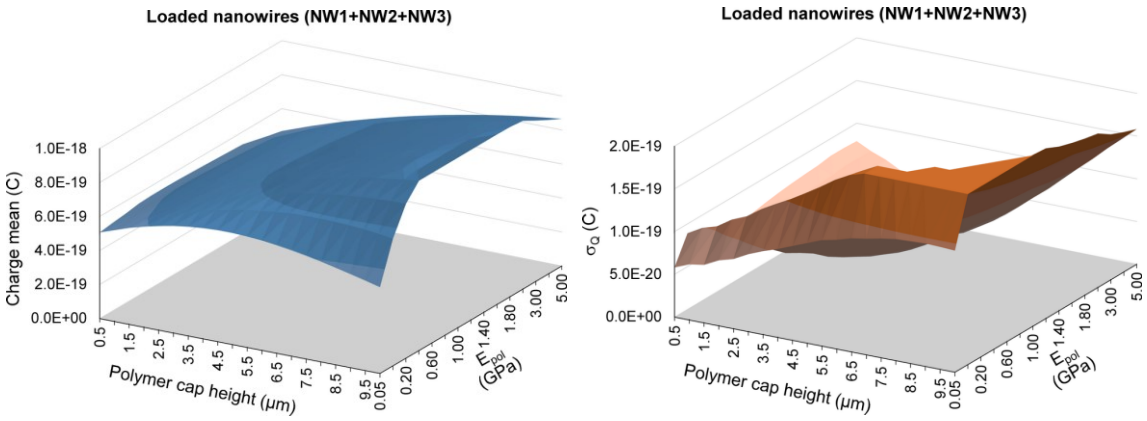

(a) (b)

Figure 3.2.2.4: Surface plots of the average charge outputs and their variability as a function of polymer cap height and Young's modulus for the case of vertical load $F_v = 1$ MPa for $AR_{NW} = 30$ ($w_{NW} = 0.5$ μm, $h_{NW} = 15$ μm).

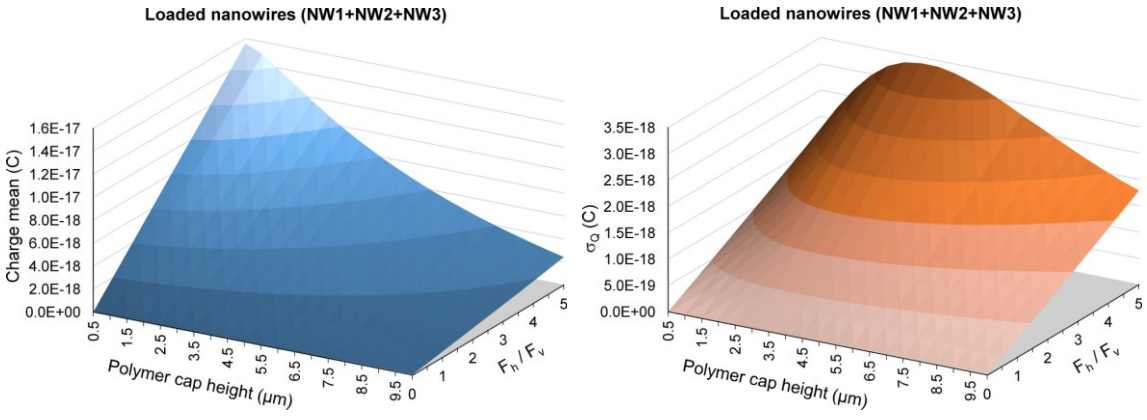

(a) (b)

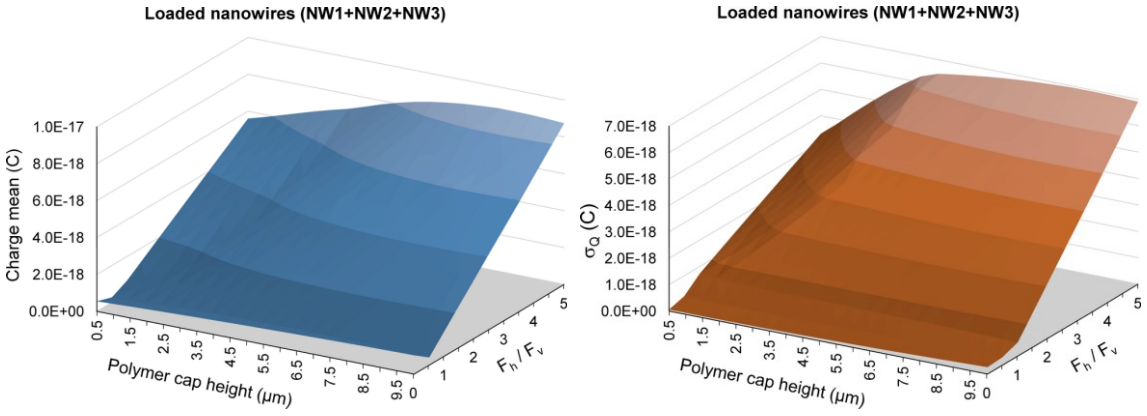

(c) (d)

Figure 3.2.2.5: Surface plots of the average charge outputs and their variability as a function of the ratio of horizontal force to vertical force for: (a)-(b) AR_{NW} = 5 (w_{NW} = 0.5 μm, h_{NW} = 2.5 μm); (c)-(d) AR_{NW} = 30 (w_{NW} = 0.5 μm, h_{NW} = 15 μm). E_{pol} = 0.5 GPa.

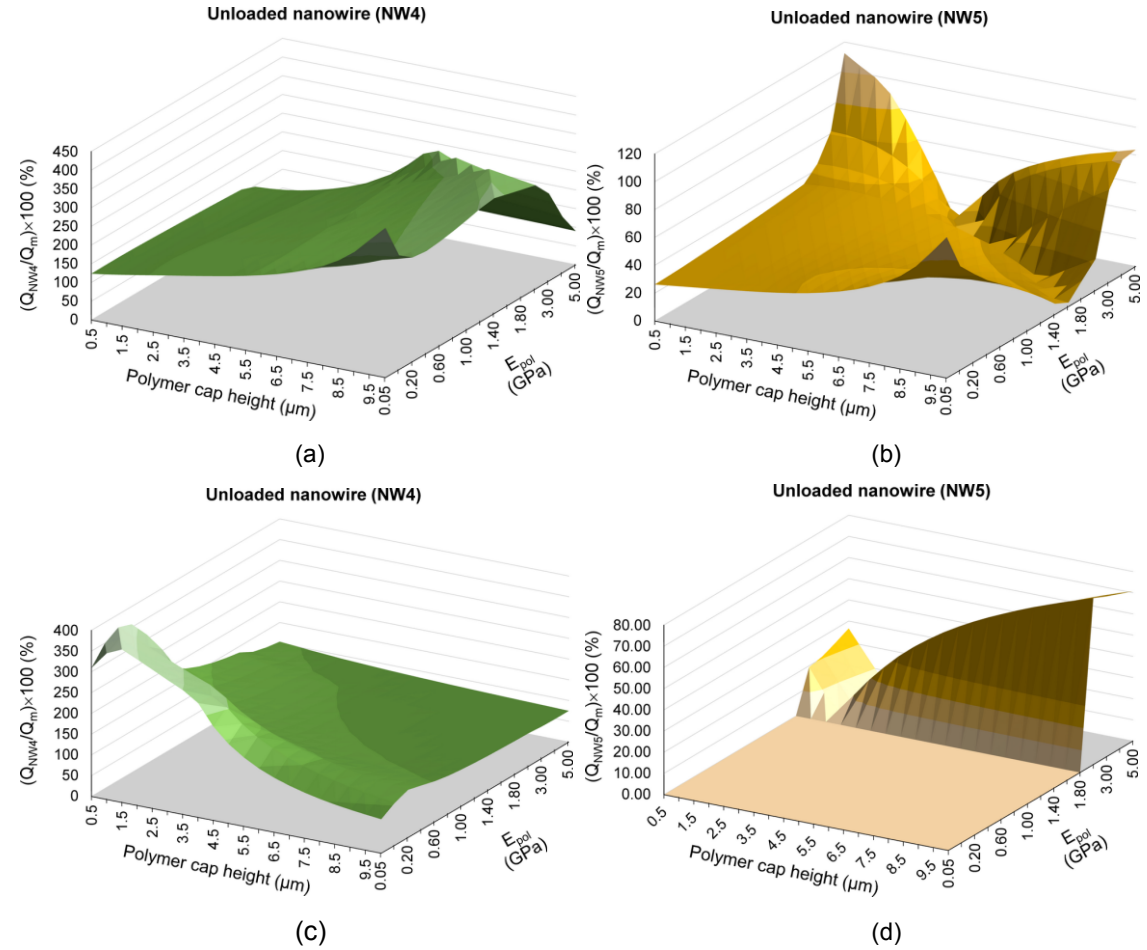

(a) (b)

(c) (d)

Figure 3.2.2.6: Surface plots of spurious signals as a function of polymer cap height and Young's modulus for the case of oblique load $F_h = F_v$ = 1 MPa for: (a)-(b) AR_{NW} = 5 (w_{NW} = 0.5 μm, h_{NW} = 2.5 μm); (c)-(d) AR_{NW} = 30 (w_{NW} = 0.5 μm, h_{NW} = 15 μm).

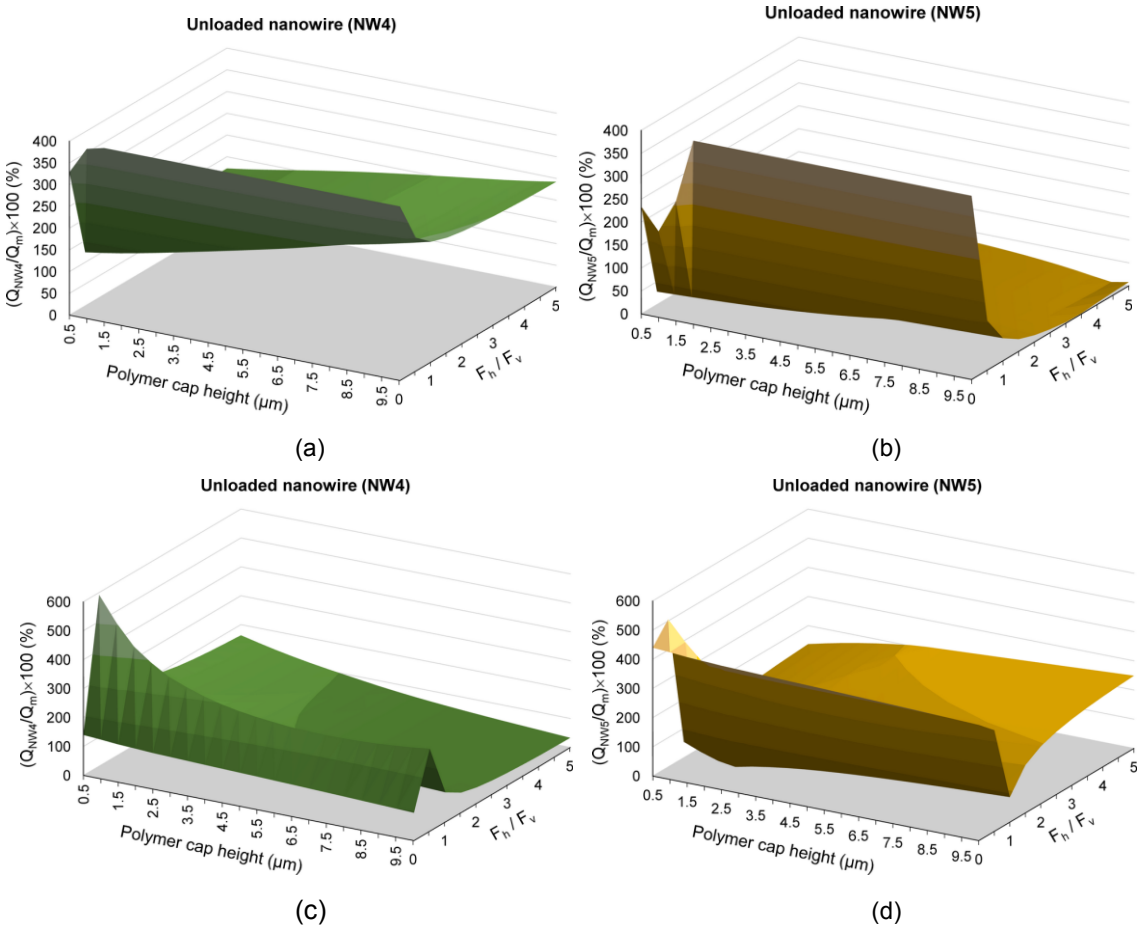

Figure 3.2.2.7: Surface plot of NW4 and NW5 charge outputs as a function of the ratio of horizontal force to vertical force for: (a)-(b) AR_{NW} = 5 (w_{NW} = 0.5 μm, h_{NW} = 2.5 μm); (c)-(d) AR_{NW} = 30 (w_{NW} = 0.5 μm, h_{NW} = 15 μm).

Parametric study was also performed in order to predict the near-optimal values of polymer Young's modulus E_{pol} and cap height h_{pol} in terms of the strain-induced (piezoelectric) charge outputs. It was done by examining 3D plots, which were derived for low and high aspect ratio NWs when the array was deformed by the pressure load of varying orientation (Figures 3.2.2.3-3.2.2.5). Similarly to the case of voltage outputs, the charge outputs also undergo more complex variation with changing E_{pol} and h_{pol} when the horizontal load component is introduced and when NW aspect ratio is increased. Comparison of the mean charge plots (Figure 3.2.2.3) reveals that bending stiffness of the NWs (determined by the aspect ratio) has a significant impact on the charge outputs and their variability. The observed complex dependence on the load orientation and NW aspect ratio makes it challenging to unambiguously identify the near-optimal values of E_{pol} and h_{pol} since the character of the pressure load in real life will change from person to person. Thus, the recommendation for the near-optimal values is based on the assumption that in majority of cases there will be at least some horizontal load component during the actual fingerprint sensor usage. Therefore, in order to be on the safe side, the recommended values of near-optimal E_{pol} and h_{pol} are:

- For low aspect ratio NWs (AR_{NW} = 5): the lowest possible values, i.e. $E_{pol} \approx$ 0.05 – 0.2 GPa, $h_{pol} \approx$ 0.5 – 2 μm. At these values the spurious signals are minimized (Figure 3.2.2.6a-b).
- For high aspect ratio NWs (AR_{NW} = 30): 0.2 ≤ E_{pol} ≤ 2 GPa, 4 ≤ h_{pol} ≤ 6 μm. At these values the spurious signals are minimized (Figure 3.2.2.6c-d).

Numerical results reveal (Figure 3.2.2.6-3.2.2.7) that the spurious signals for Option 2 NW array have considerably larger values with respect to the mean charge output values (i.e. useful signals). This suggests that Option 2 fingerprint sensor could have lower native spatial resolution in comparison to the analogous Option 3 sensor (i.e. if it is assumed the piezo-pixel of Option 3 sensor consists of a single NW, and not the NW bundle as is the case for PoC3/DEMO3). Overall, Option 2 NW array exhibits more complex electromechanical behavior when subjected to varying input parameters.

3.3 Piezo-semiconductive chip-based model of the encapsulated Option 2 ZnO NW array (ver. FEM2.3)

3.3.1 Model implementation

Piezo-semiconductive chip-based model ver. FEM2.3 was implemented in the same manner as the aforementioned model ver. FEM3.4. The model is adaptive and can be easily extended to the multi-NW configuration if array-related phenomena had to be analyzed (as in the case of models ver. FEM2.2).

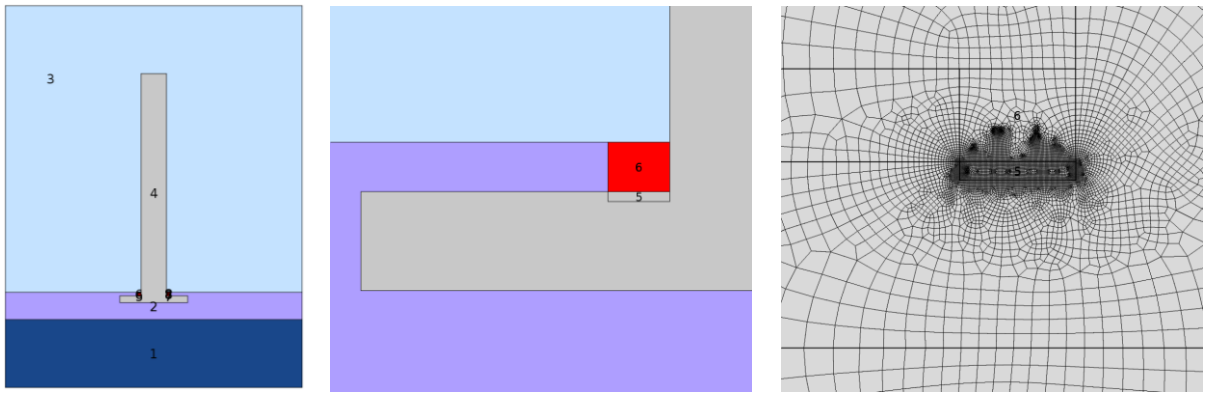

Figure 3.3.1.1: (a) Piezo-semiconductive chip-based model (ver. FEM2.3) of the encapsulated Option 2 ZnO NW (with Schottky contacts between the side electrodes and ZnO seed layer), corresponding to PoC2 realized and tested by MTA. (b) Close-up view of the left side of seed layer (1,2,3 – dielectric medium (Si, SiO_2 and polymer, respectively), 4 – ZnO NW with seed layer, 5 – depletion region, 6 – gold electrode). (c) Close-up view of the seed layer with very finely meshed depletion region and its surroundings.

In this case, the modeled configuration (Figure 3.3.1.1) essentially corresponds to the PoC2, which was developed and tested by the MTA. Namely, gold side electrodes are directly contacted at the bottom to the seed layer where they form Schottky contacts (both in the case of left electrode (terminal) and right electrode (ground)). Electrical contacting of the electrodes to the side surface of the NW at its root was neglected in this case, though it can be easily added if required.

3.3.2 Results of numerical studies and experimental verification

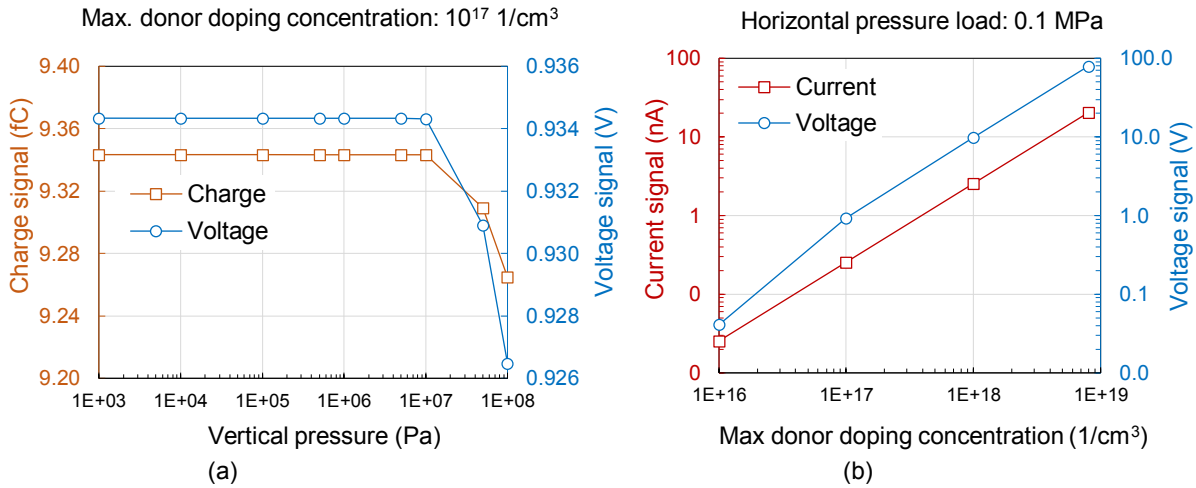

Figure 3.3.2.1: Representative numerical results obtained with the piezo-semiconductive chip-based model (ver. FEM2.3) of the encapsulated Option 2 ZnO NW (with Schottky contacts between the side electrodes and ZnO seed layer) corresponding to PoC2 realized and tested by MTA. The plots show variation of electrical signals as a function of vertical pressure (a) and maximum donor doping concentration in ZnO (b). Model properties: NW width – 0.75 μm, NW length – 6.443 μm, external capacitor connected to NW – 10 fF.

Analogously to the simulation case reported in Section 2.3.2 for the model ver. FEM3.4, the developed piezo-semiconductive PoC2 model was also subjected to parametric studies: Figure 3.3.2.1a – changing the magnitude of pressure load (acting horizontally since PoC2 is intended for bending force sensing) and maintaining the maximum donor doping concentration constant (10^{17} 1/cm^3) and Figure 3.3.2.1b – changing the concentration at the fixed horizontal pressure load (0.1 MPa).

Conducted numerical studies indicate the following:

- Similarly to the Option 3 case (Figure 2.3.2.1a) with vertical pressure load, in the PoC2 case with horizontal pressure load we may observe low- and high-load ranges in terms of trends of variation of electrical signals (Figure 3.3.2.1a), though in the latter case the low-load range is extended up to higher load levels (~10 MPa).
- In low-load range (roughly: <10 MPa) the electrical signals: a) have relatively high magnitude that cannot be attributed to the strain-induced piezoelectric effect, b) are insensitive to the increasing horizontal load. In high-load range (roughly: >10 MPa) the charge and voltage signals become very weakly sensitive to the increasing load. Strain-induced voltage and charge sensitivities in high-load range reach only 8.5×10^{-2} μV/kPa and 8.5×10^{-7} fC/kPA, respectively (it is about 40 times lower in comparison to the Option 3 case reported in Section 2.3.2).
- In contrast to Option 3 case, the current signal is constant throughout the whole load range and does not exhibit any strain-dependency whatsoever. Thus, it is impossible to compare PoC2 and PoC3 in terms of their strain-induced current densities. However, both architectures may be compared in terms of their total current output. In this case it is interesting to note that PoC2 outperforms PoC3 since its current density is about 18 times larger (5.77×10^{7} nA/cm^2 for PoC2 vs. 3.15×10^{6} nA/cm^2 for PoC3 (at maximum donor doping concentration of 10^{17} 1/cm^3)).
- Analogously to the Option 3 case, electrical signals strongly depend on the maximum donor doping (n-type) concentration in ZnO (Figure 3.3.2.1b): the most pronounced increase is predicted in the range of 10^{18} – 8×10^{18} 1/cm^3. Predicted current signal at 10^{18} 1/cm^3 reaches a couple of nA, which is in good agreement with the experimental values observed by MTA during in-situ current measurements with the polymer-coated PoC2 samples.

3.4 Summary

Main results of the numerical studies for Option 2 NW array are as follows:

- Using the multi-NW piezoelectric model of the encapsulated Option 2 ZnO NW array (ver. FEM2.2):
  - The most rational (near-optimal) values of Young's modulus and thickness of the encapsulating polymer layer were established in order to maximize electrical signals generated by the piezoelectric NWs, which would facilitate the detection and post-processing of the signals.
  - The average piezoelectric signals exhibit more complex variation with changing polymer Young's modulus and cap height when horizontal load component is present and when NW aspect ratio is increased.
- Using the piezo-semiconductive chip-based model of the encapsulated Option 2 ZnO NW array (ver. FEM2.3):
  - In low-load range (roughly: <10 MPa) the electrical signals: a) have relatively high magnitude that cannot be attributed to the strain-induced piezoelectric effect, b) are insensitive to the increasing bending force. In high-load range (roughly: >10 MPa) the charge and voltage signals are very weakly sensitive to the increasing load (current is not sensitive at all).
  - It is predicted that in terms of total current output (not force-dependent!), PoC2 outperforms the PoC3 since the current density of the former is about 18 times larger with respect to the latter.
  - Magnitude of electrical signals strongly depends on the maximum donor doping concentration in ZnO. Current signal at 10^{18} 1/cm^3 is on the order of several nA, which is in good agreement with the experimental results reported by MTA for their polymer-coated PoC2 samples.